Studies on 3D Printed Nanocomposite Gel Polymer-Based Electrolyte for Li-ion Batteries

BY

MASSIMILIANO MASTROGIORGIO
B.S., Politecnico di Torino, Turin, Italy, 2019

THESIS

Submitted as partial fulfillment of the requirements
for the degree of Master of Science in Mechanical Engineering
in the Graduate College of the
University of Illinois at Chicago, 2021

Chicago, Illinois

Defense Committee:

Reza Shahbazian-Yassar, Chair and Advisor

Vitaliy Robert Yurkiv

Andrea Lanzini

Marco Masoero, Politecnico di Torino

ACKNOWLEDGMENTS

Before I start, I would like to express my appreciation to my family. Without youI would not be here, in Chicago, pursuing my higher education. I am forever thankful for the constant support and guide that you gave me every day throughout this project.

I would also like to thank Prof. Masoero, who represents my home university, Politecnico di Torino, for the support that I received during the different phases of the project.

Thank you to Prof. Shahbazian-Yassar, who let me join his high-level research team. Working in his Lab allowed me to grow both professionally and personally.

A special thank you to Vahid and Golam, who directed me during this 6 months of research, two friends more than lab colleagues.

I aspire to work with this magnificent team and be part of future collaborations. I am grateful for the immense opportunity granted to me..

M.M

TABLE OF CONTENTS

iii

LIST OF TABLES

LIST OF FIGURES

LIST OF FIGURES (continued)

LIST OF FIGURES (continued)

LIST OF ABBREVIATIONS

3D	Three dimensional
RFID	Radio frequency identification
h-BN	Hexagonal Boron-Nitride
LCO	Lithium Cobalt Oxide
PAN	Polyacrylonitrile
PMMA	Polymethylmethacrylate
PVC	Polyvinyl Chloride
PVDF	Polyvinylidene fluoride
NMP	N-Methyl-2-pyrrolidone
G'	Storage modulus
G''	Loss modulus
DIW	Direct ink writing
EV	Electric vehicles
ISC	Internal short circuit
BMS	Battery management system
HTR	Heat-Temperature-Reaction
Emim – TFSI	1-Ethyl-3-Methylimidazolium Bis (Trifluoromethylsulfonyl)imide
LiTFSI	Bis(trifluoromethanesulfonyl)imide
CE	Coulombic efficiency

SUMMARY

Recent developments in the field of mobile application and transport have heightened the need for efficient energy storage systems. Batteries are the most widespread energy storage systems for powering portable electronic devices and electric vehicles. Between them, the most used type of battery is Lithium-ion batteries. 3D printing of Li-ion batteries also known as secondary type batteries received vast recognition for advancing the next generation of 3D energy storage devices. Printing technologies offer simple processing and low-cost manufacturing, resulting in the potential replacement of conventional technologies.

This thesis project is focused on the synthesis of a printable polymer-based electrolyte for Li-ion battery with a relative study of the 3D printing process, electrochemical and thermal properties of the electrolyte. The Poly(vinylidene fluoride-hexafluoropropylene) matrices and a Li+-conducting ionic-liquid salt are components of the hybrid polymer-based electrolyte developed in this study. To attain the desired rheological qualities of the electrolyte solution and improve the thermal properties of the electrolyte, the electrolyte ink composition was modified by adding Silane Boron-Nitride nanosized ceramic filler. Once verified the effective printability of the ink, a detailed analysis of the influence of the 3D printing machine dispensing parameters on the final printed structure was conducted. The overpotential and cyclability tests, performed to characterize the electrochemical properties, revealed interesting performances of the printed polymer electrolyte. Finally, the electrolyte enhanced thermal properties were demonstrated with a direct comparison between the 3D printed polymer electrolyte and a common liquid electrolyte.

Nevertheless, further studies regarding the safety of the electrolyte can help to better understand the thermal runaway mechanism and serve as a source of inspiration for future work.

1 INTRODUCTION

1.1. Motivations

The worldwide diffusion of portable electronic products such as laptops, hand-held computers, mobile phones, and camera devices is leading to a rise in demand for energy storage systems [1]. Furthermore, energy storage devices are becoming increasingly important for capturing the energy supplied by intermittent renewable energy sources including photovoltaics, wind, and geothermal. [2]. The transfer of electrical energy from a power source into a form that may be kept for later conversion back to electrical energy is known as electrical energy storage. [3]. Due to the larger amounts of energy collected, batteries are commonly employed as energy storage systems, particularly for portable electronic equipment. [4]. One of the most used battery types is lithium-ion batteries, with a market share of 75% [5]. A battery is characterized by three basic components: cathode, anode, and separator/electrolyte; the electrolyte assists to complete the redox processes within the cell by providing ionic contact between the electrodes. [6]. Improvements in electronic conductivities and ionic diffusivities in anode, cathode, and electrolyte materials continue to be attainable in the field of lithium-ion batteries. [7].

Advances in the field of batteries incorporating printed technologies are expected to assist the expanding field of small portable and wearable electronic devices for applications such as smart cards, remote sensors, and medical equipment. This arose from the development and spread of smart and functional materials, as well as microelectromechanical systems that required an onboard power supply with 5 to 10 mAhcm^{-2} capacities with a 10 mm^2 total size [8], [9]. Printed batteries can bridge the gap for small portable devices where size, weight, and increased device integration are all important factors. The research community started to explore new electrolyte compositions suitable for printed batteries, passing from a liquid-based electrolyte to gel- and

solid-state polymer electrolytes to solve safety issues related to liquid-based electrolytes and improve the electrochemical and mechanical performance of the gel- and solid-state polymer electrolytes.

Hexagonal boron nitride (h-BN) materials, with outstanding thermal conductivity, have attracted enormous interest in the scientific community. h-BN materials are considered to be promising fillers to improve the mechanical and thermal properties of gel-based electrolytes [10].

1.2. Objectives

The project aims at validating a 3D printed gel-like polymer electrolyte, which has thermal enhanced performance due to the Silane Boron-Nitride additive. To characterize the novel polymer electrolyte, mechanical, electrochemical, and thermal tests were performed to consistently demonstrate the possibility of commercial application of 3D printed Lithium-ion battery electrolyte, with particular attention on safety, durability, and manufacturing aspects.

2 THEORY

2.1. Brief overview Li-ion battery

The transfer of lithium ions and electrons between two electrodes powered lithium-ion batteries. Li^+ ions move from the positive electrode towards the negative during charge, and in the opposite direction when discharging. The negative and the positive electrodes are traditionally called anode and cathode. With respect to batteries made from other materials such as zinc and lead, lithium-ion batteries have higher specific energies due to the relative lightweight and low density of lithium [11]. The most common cathode material for commercialized Li-ion batteries is LCO, whereas graphite is largely used as the anode. The neutral lithium is oxidized and turned to Li+ at the negative electrode. These Li^+ ions subsequently travel to the cathode, where they combine with $LiCoO_2$ to form $LiCoO_2$. When electrons from the anode reaction reach the cathode, they reduce Co(IV) to Co(III). The battery can be recharged by conducting the reactions in reverse because lithium is involved in both electrode processes. During discharge, lithium is oxidized from Li to Li^+ in the lithium-graphite anode through the following reaction:

$$C_6Li \rightarrow 6\ C + Li^+ + e^- \qquad (2.1)$$
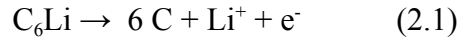
These lithium ions migrate through the electrolyte medium to the cathode, where they are incorporated into lithium cobalt oxide through the following reaction, which reduces cobalt from a +4 to +3 oxidation state:

$$LiCoO_2 \rightarrow Li_{1-x}CO_2 + x\ Li^+ + x\ e^- \qquad (2.2)$$

3
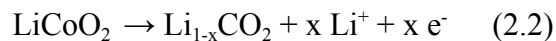
Where 0 < x < 0.5. These reactions can be run in reverse to recharge the cell. In this case, the lithium ions leave the lithium cobalt oxide cathode and migrate back to the anode, where they are reduced back to neutral lithium and reincorporated into the graphite network. To allow the Li ions to move back and forth, it is essential to have an electrolyte that closes the circuit. For the electrolyte, materials with high ionic conductivity are largely used in order to facilitate the process [12]

Salts, solvents, and additives make up the electrolyte. The salts provide a pathway for lithium ions to flow, the solvents dissolve the salts, and the additives are provided in minute amounts for specialized functions. Different types of electrolytes can be used in Li-ion batteries, however, liquid electrolytes are generally used and commercialized for many reasons. One of the main features of a liquid electrolyte is the good performances that they can provide and the ease of manufacturing with respect to gel or solid materials. One of the most common ones is $LiPF_6$, which has outstanding properties at ambient temperature [13]. Although, it can be very unsafe in some circumstances. In fact, a great concern is the thermal instability that lets it decompose at 80°C, producing PF_5 [14]. This gaseous is very reactive and in the presence of moisture or water forms HF and POF_3 which are further reactive. Those reactions usually degrade the battery leading to fire or explosion [14]–[16]. Battery safety is an increasing concern to guarantee consumer safety. For these reasons, the scientific community is moving forward and gel- and solid-state electrolytes have been developed to meet the required safety standards. The main challenge is realizing an electrolyte with high-performing essential parameters such as ionic conductivity and ionic diffusion, but, at the same time, able to guarantee sufficient safety properties.

2.2. Polymer electrolytes for Li-ion battery

Polymer electrolytes have been suggested as a possible alternative to liquid electrolytes. Nonetheless, the majority of the polymer electrolytes studied had a number of drawbacks that limited their commercial viability. [17]. On the other hand, among other non-liquid electrolytes, they have the advantages of being higher ionic conductors and mechanically flexible. Polymer electrolytes can be used in different applications due to their unique mechanical properties. Gel polymer electrolytes are made out of a polymeric membrane with a salt-solvent mixture added to it. The solvent serves as a plasticizer, causing the polymer matrix to expand, resulting in a change in physical appearance from solid to gel. The "gellification" enhances the interfacial contact with the electrodes in comparison to solid-state electrolytes [18]. The most popular polymers used to prepare Gel polymer electrolytes are polyvinylidene fluoride (PVDF), polyacrylonitrile (PAN), polyvinyl chloride (PVC). Polymers, which strongly interact with solvent, tend to form very stable gels, but these are characterized by very poor mechanical properties. For this reason, the choice of a particular polymer matrix is very important. The polymer electrolyte must have appropriate ionic conductivity to let the ions be transported along with the structure and reach the electrodes, and electrochemical, thermal, and mechanical stability over a wide temperature range is required [19]. An important aspect to take into consideration is the electrode-electrolyte interface characteristics. It is important to maximize the interface characteristic in order to not have a supplementary resistance, which would lead to overpotential losses. On the other hand, ease of preparation for future manufacturing purposes is extremely important for the commercialization of energy storage devices based on polymer electrolytes.

The studied polymer matrix is composed of a mixture of PVDF and NMP. An essential requirement for the electrolyte is the need to have a high dielectric constant. A high dielectric constant is necessary for both the salt dissociation and having low electronic conduction [20], [21]. To obtain the desired value for the dielectric constant and the desired electrolyte viscosity, a detailed study on the polymer electrolyte composition must be performed [22].

Lithium salt and ionic liquid also play a crucial role in the final performance of the electrolyte. The lithium salt must have some peculiarity like [14]:

o   High ionic conductivity to enhance the ion conduction throughout the polymer structure

o   Thermal and chemical stability in the range of the operating conditions to ensure higher safety and reliability

o   Form less-resistive SEI on the electrodes for guaranteeing long-term cyclability

Concerning the ionic liquid, it is often used for the synthesis of electrolytes. Ionic liquids are salts that are liquid at room temperature. They present unique properties such as non-flammability, goof ionic conduction, high thermal stability over a wide temperature range, and outstanding electrochemical behavior over wide electrochemical windows [23].

2.3. Ion transport mechanism

Low ionic conductivities at ambient temperature and poor stabilities for gel- and solid-electrolyte have slowed down the diffusion of commercial application of all-solid-state lithium-ion batteries [24]. The ionic conductivities of liquid electrolytes at room temperature are higher than those of solid electrolytes. The majority of solid electrolytes are unstable against negative electrodes at low potential, while some are reactive towards cathode materials, resulting in significant interfacial resistance. [25].

The Li-ions have three transport mechanism within a polymer matrix [26]:

- The segmental motion of coordinated ions

- The intrachain motion of ions along the polymer backbone

- Intersegmental hopping of ions from one polymer chain to another

In different types of electrolytes, one is more likely to occur than others, even if usually they are all present. It is worthy to underline that the segmental motion occurs above the glass transition temperature and in amorphous regions [27]. Gel electrolytes are characterized by a large portion of amorphous regions with respect to their solid counterparts.

2.4. 3D printing technologies

Conventional batteries present four main designs: cylindrical, prismatic, spiral wound, and coin cell. The four designs are bulky and rigid, not applicable for flexible electronic devices. Printed batteries cannot compete with conventional batteries in application with no size and shape limitations, but They can bridge the gap for small portable devices, where size, weight, and increased device integration are all important factors. The most valuable features and attributes of printed batteries are mechanically flexibility, high power, low cost, customizability, and rechargeability [28].
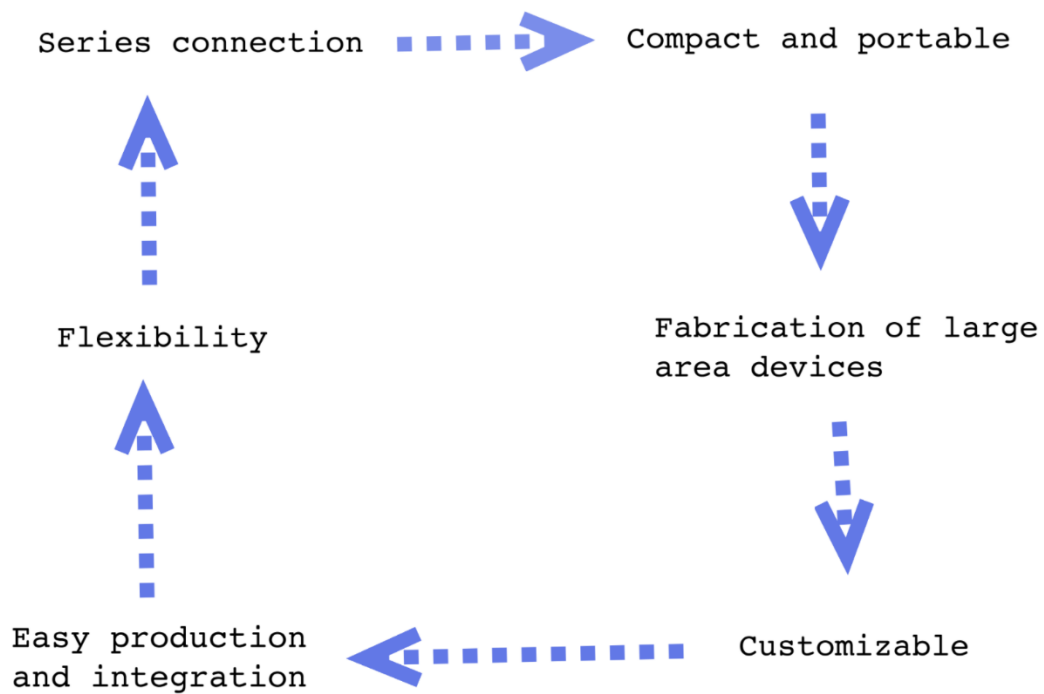
FIGURE 1. MAIN ADVANTAGES OF PRINTED BATTERIES

Eco-friendly solutions related to the processes of fabrication and used materials can be implemented.
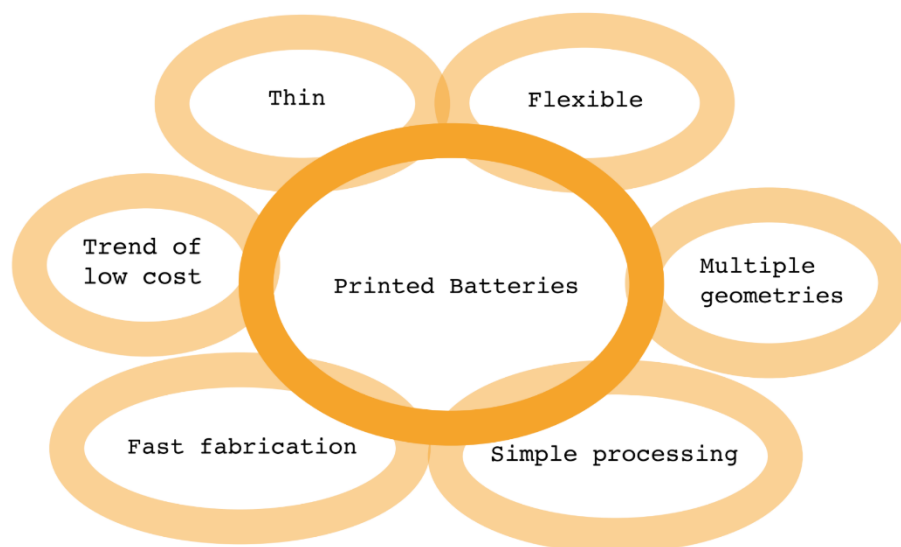
FIGURE 2. MAIN FEATURES AND ATTRIBUTES OF PRINTED BATTERIES

Additive manufacturing, often known as 3D printing, is a new technology for producing objects with multiple structures and complicated designs [29]. Direct ink writing (DIW) is a viable technology for producing next-generation batteries with complex microstructures and good performance. Low-cost fabrication processes and simple printing mechanisms are two of the main advantages of the implementation of this technique. One of the challenges is the development of inks for printing battery components such as electrodes, electrolytes, and separators. Ionic conductivity and mechanical and thermal stability are required for printing solid-state electrolytes.

The efforts and challenges in printing high aspect ratio designs are centered on optimizing the ink composition and rheology to allow reliable flow through fine deposition nozzles, enhance adhesion between printed components, and offer the appropriate structural qualities. [30]. The way materials deform or flow in response to applied forces or stresses is described by rheological

characteristics. [31]. The rheology of the ink plays a crucial role in the printability of the electrodes or electrolytes. Detailed analysis is performed on the apparent viscosity, storage, and loss moduli of the slurry. Shear-thinning behavior is a must-have property of the ink. The viscosity of the fluid decreases as the shear increases during shear-thinning. Rearrangements in the fluid microstructure in the plane of the applied shear induce shear thinning. [32]
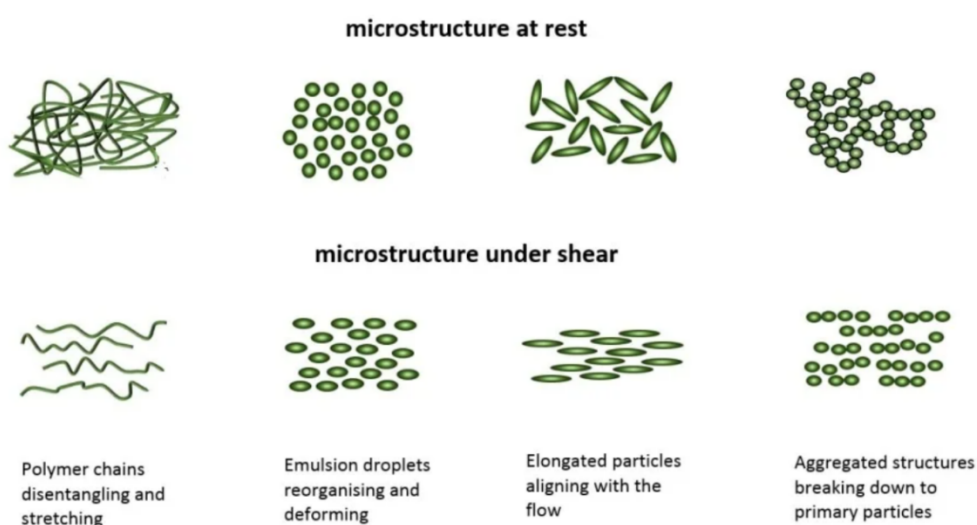
FIGURE 3. DIFFERENT MICROSTRUCTURE RESPONSE TO SHEAR APPLICATION

The loss and storage moduli of the component slurry are also important. The storage modulus (G') provides insight into the structure of a material. It represents the energy stored in the sample's elastic structure. The loss modulus (G") tells us about the viscous fraction of the energy dissipated in the sample [33]. If the storage modulus is greater than the loss modulus, the sample should be able to return to its original configuration to some extent, whereas if the loss modulus is greater than the storage modulus, the sample microstructure collapses and the mechanical energy imparted to the material is dissipated, causing the material to flow. Cheng et al. created a

solid-state electrolyte ink and engineered an elevated-temperature DIW 3D-printer from a robotic deposition to enable 3D printing of hybrid solid-state electrolyte batteries. In the graphs below, the rheological properties of the electrolyte ink are displayed.
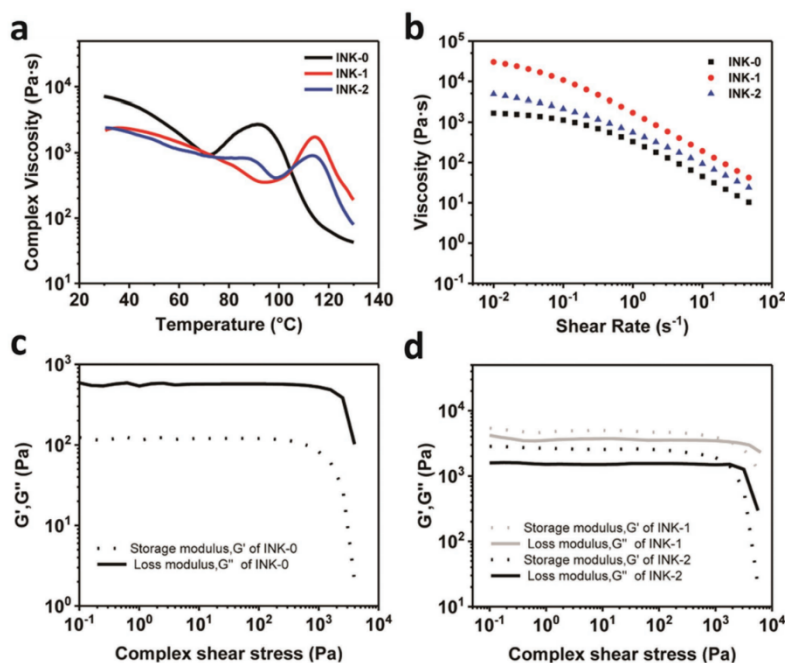
FIGURE 4. PROPERTIES OF THE POLYMER ELECTROLYTES INK

INK-0 denotes a polymer electrolyte without ceramic fillers, while INK-1 and INK-2 signify nanocomposite electrolytes with 2.5 and 5 wt% TiO2, respectively. Shear-thinning behavior can be seen in all of the inks. INK-1 and INK-2 have higher viscosity values than INK-0, indicating that nanoparticles are to blame for the increased viscosity. In terms of storage and loss modulus, the loss modulus is bigger than the storage modulus for ink without fillers (INK-0). This means that the INK-0 behaves as a liquid in the range of 0.1 to 10^4 Pa. While this enables for easier ink extrusion through the nozzle during printing, the lower storage modulus at low shear stress

means that the printed ink cannot be appropriately stacked to form high-quality 3D structures while the nozzle is moving. In comparison to INK-0, the inks with fillers behave differently at 10^{-1} to 10^3. The inks' storage moduli are larger than their loss moduli in this location, indicating a solid-like characteristic that is advantageous for solidification during 3D printing. In the high shear stress zone after the yield point, the inks behave like liquids. This means that during printing, the inks containing additives flow into the syringe and disperse via the nozzle [34].

This is an example of the crucial role played by nanoscale additives for the manufacturing of 3D printed batteries.

2.5. Effect of nanoscale additive

A promising approach to increase the level of amorphicity in polymers is to add solid additives such as SiO2 or TiO2. These components can improve ionic conductivity and reduce the formation of crystals. The nanoparticles may act as cross-linking centres for PVDF chain segments which destabilize the coordination around the cations and interfere within the cations and anions interaction promoting salt dissociation [35]. The mobility and the concentration of free ions enabled by nanocomposites are two positive effects that have been observed in the field of material engineering. Due to their size, nanocomposites are more active and effective and can modify the properties of their polymers. The possibility to tailor the properties of the nanocomposite materials has increased the researchers' interest over the years.

2.6. Thermal runaway

The safety concern is one of the main obstacles to the large-scale application of lithium-ion batteries in a different field such as electric vehicles. Thermal runaway is the key scientific

problem in battery safety research [36]. The thermal runaway process occurs because of abuse conditions:

o   Mechanical abuse

o   Electrical abuse

o   Thermal abuse

The process follows a mechanism of chain reaction, during which a chemical reaction or other process promotes or spreads the reaction, which under certain conditions may accelerate dramatically.
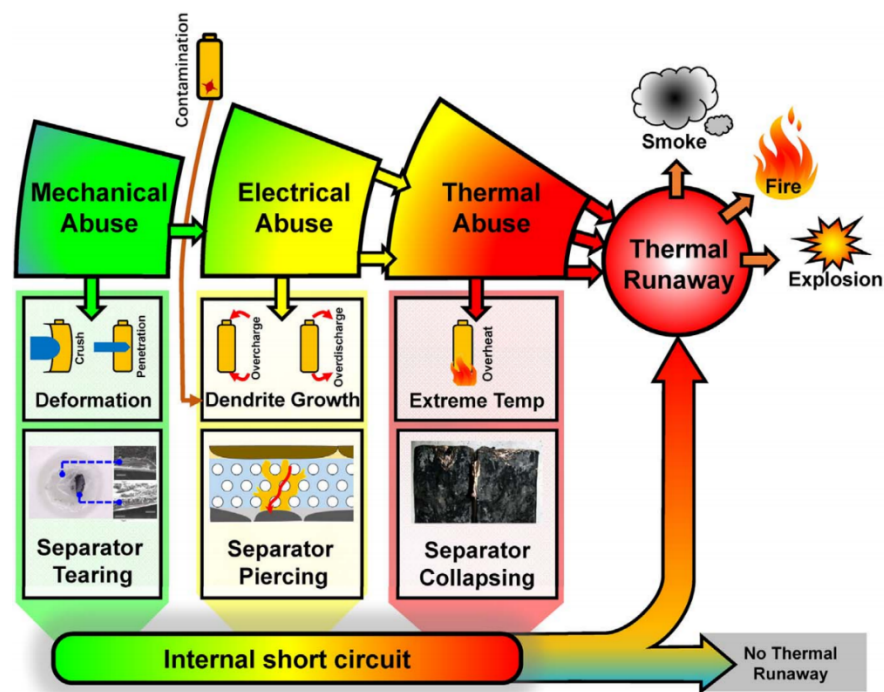
FIGURE 5. ACCIDENTS RELATED WITH LITHIUM-ION BATTERY FAILURE, AND CORRELATED ABUSE CONDITIONS

During the last ten years, several accidents of lithium-ion battery failure occurred [37]. Most of the more catastrophic involved electric vehicles (EV).

The EV production and the demand for lithium-ion battery for EV in China are displayed in the following graph.
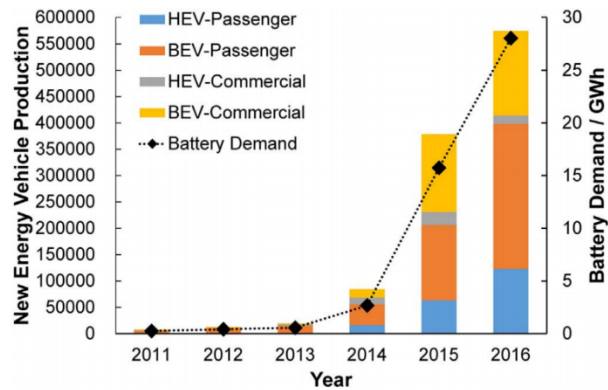
FIGURE 6. THE EV PRODUCTION AND THE DEMAND OF LITHIUM-ION BATTERY FOR EV IN CHINA

As it is possible to understand from the graph, from the year 2015, the production of EVs has increased in a significant way. Consequently, battery fire accidents occurred more frequently.

The most common features during the accident of lithium-ion batteries are the thermal runaway and thermal runaway-induced smoke, fire, and even explosion [36]. For these reasons, many countries require the lithium-ion battery to pass mandatory tests, before its application in EV. However, accidents involving thermal runaway still sporadically occur. The main reasons are:

o   Probability of self-induced failure

o   Abuse condition in practical use

The self-induced failure rate can be calculated by the following equation:

$$P = 1 - (1 - p)^{m-n} \qquad (2.3)$$

Where:

- o   p is the self-induced failure rate

- o   m is the number of EVs

- o   n is the number of the cells within its battery pack

- o   P is the failure rate

Taking as an example Tesla Model S, assuming a self-induced failure rate p of 0.1 ppm, m equal to 1000, and n equal to 18650, the failure rate P is 0.9992, indicating that the failure rate is approximately 1 over 10000 [36].

On the other hand, it is more complicated to establish a correlation to predict the failure of the battery due to abuse conditions in practical use. The abuse conditions can be categorized into mechanical abuse, electrical abuse, and thermal abuse.

2.6.1. Mechanical abuse

It is defined as mechanical abuse of the destructive deformation and displacement caused by an applied force. One possible cause of mechanical abuse is vehicle collision with a consequent crush or penetration of the battery pack [36].

2.6.1.1. Collision and crush

The battery pack may deform after a car collision, and the design of the onboard battery pack affects the system's crash reaction [38]. Damage to the battery pack might have two potentially fatal outcomes:

- o   The battery separator tears, resulting in an internal short circuit (ISC).
- o   A flammable electrolyte leaks, perhaps resulting in a fire.

For these reasons, battery-pack required research studies from material level, cell level, to pack level. Many studies focused on how to model the crush phenomena at the cell level based on the mechanical properties of the cell components materials. In the same way, the model at the pack level can be designed in the mechanical model at the cell level.

2.6.1.2 Penetration

Penetration is another possible consequence of mechanical abuse due to vehicle collisions. In this scenario, the ISC is instantaneously triggered [36]. Penetration is regulated by mandatory test standards to simulate the ISC in abuse tests. The temperature of the cell rises as a result of the heat created during the short circuit. Until the cell is entirely discharged, the temperature rise will come to an end. No more thermal runaway will occur if the temperature does not reach a critical level. [36].

An internal short circuit or external short circuit can occur during the penetration. The current passes through the nail when an internal short circuit occurs, while an external short circuit is characterized by the current flowing through the electrodes [36]. The external short circuit takes

place when electrodes with voltage differences are connected by conductors. The overheating is produced by ohmic heat build-up during the short circuit, according to Spotnitz and Franklin [39]. Although the external short circuit is more similar to a fast-discharging method, the maximum current is restricted by the lithium-ion mass transfer speed [36].

One of the limits of the nail penetration test is repeatability. New standard test is being developed in the last few years to enhance the repeatability or to search for a substitute test approach [36].

2.6.2. Electrical abuse

The electrical abuse can be described by two main failure mechanism:

- o Overcharge
- o Discharge

Both are related to the state of charge of the battery.

2.6.2.1. Overcharge

The inability of the battery management system (BMS) to halt the charging activity before the maximum voltage is reached is directly related to the overcharge-induced thermal runaway. This kind of abuse condition is one of the most severe because excessive energy is filled into the battery during the overcharge. Two common features during overcharge are heat and gas generation. Heat generation is associated with ohmic heat and side reactions [36]. Saito [40] found that the amount of heat generated is proportional to the charging current, indicating that ohmic heat is one of the major sources of heat during overcharging. Wen et al. [41] looked at the process of overcharge and side reactions. Initially, the anode facing the dendrite grows at the

surface because of the unrestrained lithium intercalation. As a result of the lithium deintercalation, the cathode structure collapses, resulting in heat generation and oxygen release [36]. The release of oxygen accelerates the electrolyte decomposition, with significant gas production. At this point, the cell may vent due to the increase of internal pressure within the cell.

A modest overcharge does not directly lead to thermal runaway but can be the cause of capacity degradation [36]. The overcharge phenomena, as well as the discharge, are correlated to the state of charge of the battery. Ouyang et al. [42] observed that for a state of charge (SOC) lower than 120% no significant degradation process was observed, but the considerable capacity loss was observed when the cell was overcharged to 130% or higher.

2.6.2.2. Over-discharge

Another possible electrical abuse is over-discharge. During the process of over-discharge, the over delithiation of the anode causes the decomposition of the SEI. The decomposition of the SEI is correlated to gas generation like CO or CO2 [43]. New SEI will grow on the anode surface when the cell is recharged. The electrochemical characteristics of the anode are altered by the regenerated SEI [36]. The new electrochemical properties lead to a resistance increase and subsequent capacity degradation [44]. Furthermore, the cathode morphology changes during the over-discharge leading to a rapid capacity degradation [36]. Zhang et al. [45] observed that the copper collector is involved in the process. During the over-discharge process, the copper dissolves and deposits on the anode, with a consequent increase in resistance and capacity loss. The deposition of the copper can lead to ISC. The copper ions migrated through the membrane and formed copper dendrites [36]. The figure x illustrates the overall over-discharge process.
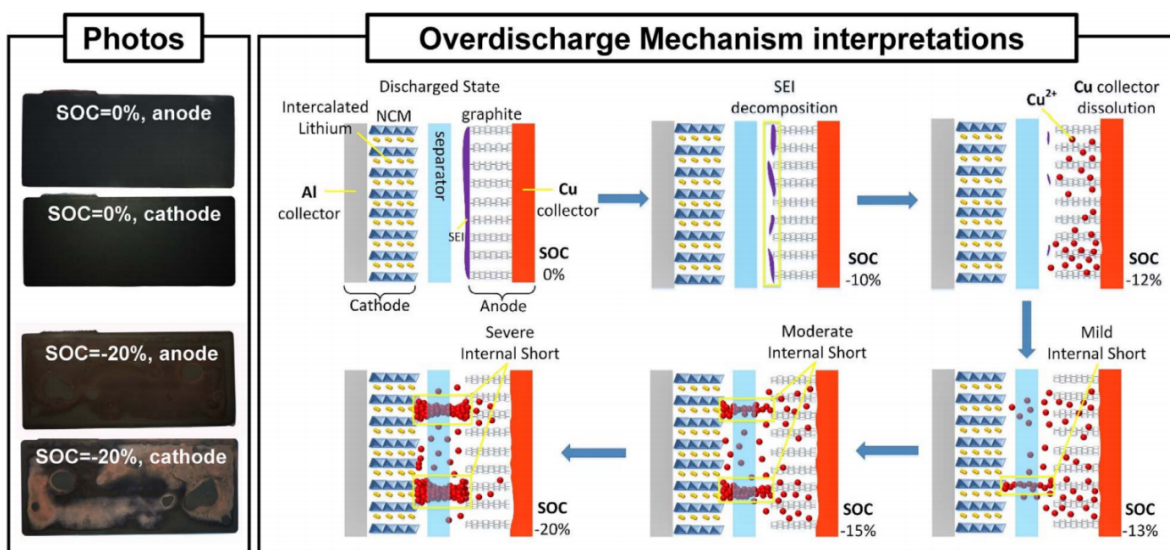
FIGURE 7. THE MECHANISM OF THE INTERNAL SHORT CIRCUIT

2.6.3. Thermal abuse

The overheating in a cell is a typical condition of thermal abuse. The overheat can be caused by contact loose of the cell collector or combustion of the automotive interior, which is correlated to an increment in contact resistance [46]. The reasons for the contact loose can be different, going from a defect during manufacturing to vibration during operation conditions [36]. When a strong current flowed through the area, it generated a lot of heat, causing local overheating and subsequent thermal runaway.

2.6.4. Internal short circuit

All the abuse conditions have an internal short circuit as a common feature. Internal short circuits happen when the cathode and anode get too close to each other due to a battery separator failure [36]. Once the internal short circuit is provoked, the electrochemical energy stored in the battery is released spontaneously as heat generation.

Mechanical and thermal abuse can immediately activate the internal short circuit, such as deformation and fracture of the separator produced by nail penetration or crush, or shrinkage and collapse of the separator with enormous internal short circuits generated by extremely high temperatures. Although not all internal short circuits will lead to thermal runaway. A mild internal short circuit can occur and generate a little amount of heat in the cell.

Because all cell products must pass matching test criteria before being sold, the likelihood of an abuse-induced internal short circuit is quite minimal [36].

However, one kind of internal short circuit cannot be regulated in the current test standard and takes the name of spontaneous internal short circuit. The spontaneous internal short circuit originated from contamination or defects during manufacturing [47].

The danger level of the internal short circuit can be evaluated by the self-discharge rate and the exotic heat generation [36]. Feng et al. proposed that there are three levels of internal short circuits.
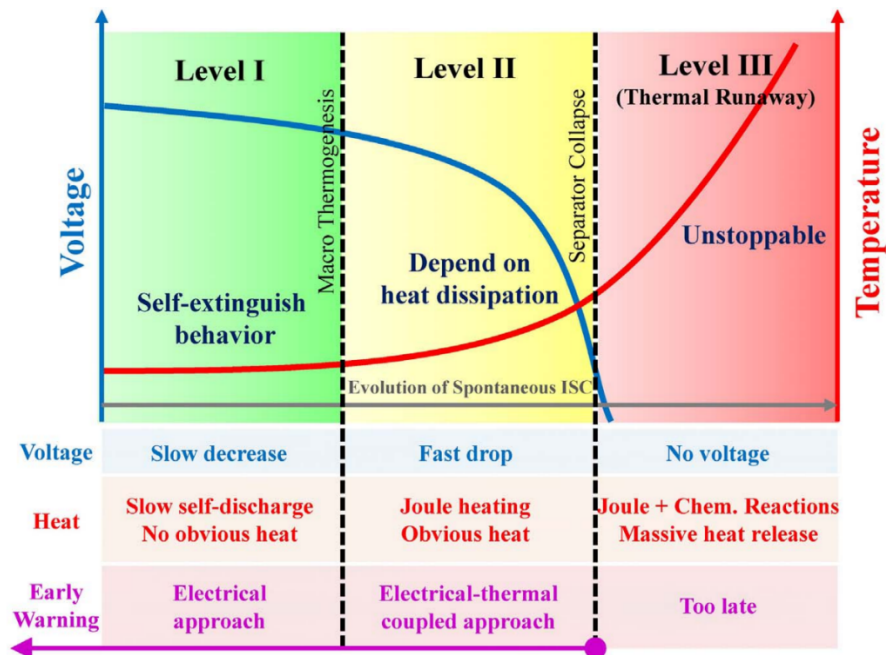
FIGURE 8. THE THREE LEVEL OF THE INTERNAL SHORT CIRCUIT

- o LEVEL I: the cell displays self-extinguish behaviour, no obvious heat generation

- o LEVEL II: a faster drop in voltage and an increase in temperature

- o LEVEL III: With extensive heat generation, thermal runaway may be uncontrollable

The battery management system (BMS) detects the malfunction and prevents permanent damage to the systems in the time it takes to progress from level I to level III.

2.6.5. Overview of the chain reactions during thermal runaway

The battery management system (BMS) detects the malfunction and prevents permanent damage to the systems in the time it takes to progress from level I to level III. The side reactions, such as

SEI disintegration, are triggered as the cell's temperature rises. In addition, the side reactions release more heat, establishing the Heat-Temperature-Reaction (HTR) loop [36].
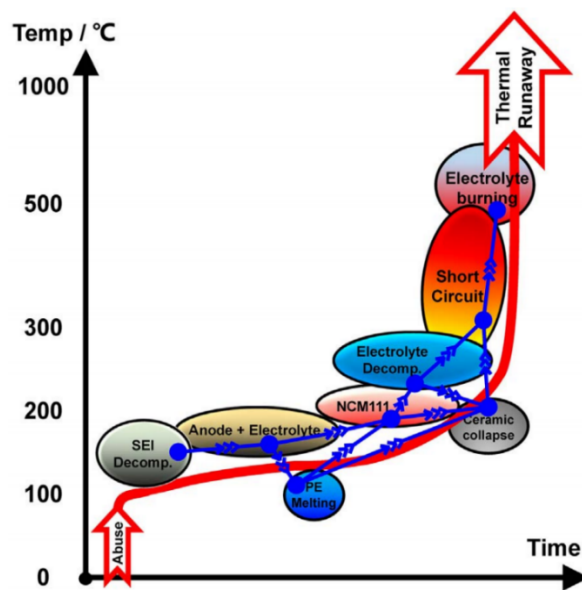
FIGURE 9. QUALITATIVE INTERPRETATION OF THE CHAIN REACTION DURING THERMAL RUNAWAY

Throughout the process, the SEI breakdown, anode-to-electrolyte reaction, separator melting, cathode fragmentation, and electrolyte decomposition were all started in the correct order.

2.6.5.1. The reaction at the anode

At the moment, the most commonly used material for lithium-ion battery anode is graphite or carbon-based material [36]. As a result, the majority of research efforts are devoted to figuring out the reaction kinetics that occur during the thermal runaway phase for carbon-based anodes [36].

A three-stage characteristic [48] can be used to explain the reaction at the graphite anode with electrolyte [48]:

1. The SEI layer's first breakdown

2. A constant rate of heat generation over a wide temperature range

3. The graphite anode's final breakdown with the electrolyte

2.6.5.2 The initial decomposition of SEI

During the thermal runaway phase, the first decomposition of SEI is the first side reaction [36]. The phenomena take place at temperature in the range of 80-120 °C [49]. The SEI decomposition can be modelled by the Arrhenius Equation:

$$\frac{dc_{SEI}^d}{dt} = A_{SEI} * c_{SEI} * \exp exp\left(-\frac{E_{a, SEI}}{RT}\right), \ (T > T_{onset,SEI}) \ (2.4)$$

Where:

- $\dfrac{dc_{SEI}^d}{dt}$ define the decomposition rate of SEI

- c_{SEI} is the normalized concentration of the SEI

- T is the temperature

- $T_{onset,SEI}$ is the onset temperature of the SEI decomposition

- A_{SEI} is the pre-exponential factor

- $E_{a, SEI}$ is the activation energy

- $R = 8.314$ j mol-1 K-1 is the ideal gas constant

Once the SEI starts disintegrating at high temperatures, the intercalated lithium in the graphite anode has the potential to touch the electrolyte.[36]. Although, the result of the interaction between the intercalated lithium and the electrolyte is the regeneration of the SEI [50].

SEI degradation and regeneration occur simultaneously in the temperature range of 120-250 °C, with the average thickness of SEI remaining constant. At the second stage, there is a modest exothermic reaction. According to Yamaki et al. [51], the wide and mild exothermic stage, as shown in figure 10, indicates the balanced reaction of SEI destruction and regeneration.
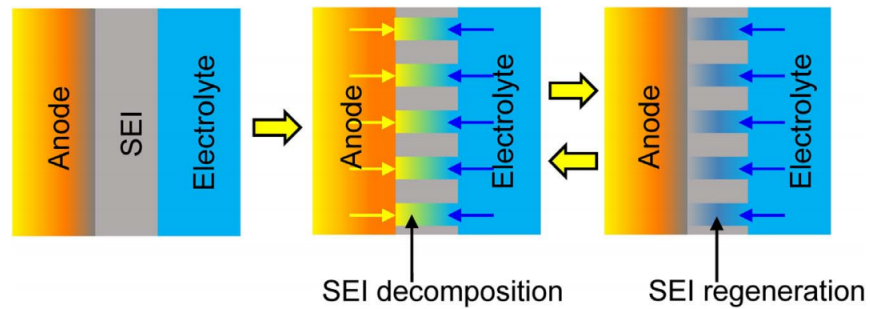
FIGURE 10. THE BALANCED REACTION OF SEI DECOMPOSITION AND REGENERATION

The entire balance process can be modelled by a set of equations, as follows.

$$\frac{dc_{SEI}}{dt} = \frac{dc_{SEI}^d}{dt} - \frac{dc_{SEI}^g}{dt} \qquad (2.5)$$

Where:

- $\frac{dc_{SEI}^d}{dt}$ is the decomposition rate and can be evaluated by eq. 1

- $\frac{dc_{SEI}^g}{dt}$ is the regeneration rate and can be evaluated y eq. 3

$$\frac{dc_{SEI}^g}{dt} = K_{SEI}^g * \frac{dc_{Li+Ele}}{dt} \qquad (2.6)$$

Where:

- K_{SEI}^g is the gain factor

- $\frac{dc_{Li+Ele}}{dt}$ is the rate of reaction between the intercalated lithium and electrolyte

$$\frac{dc_{Li+Ele}}{dt} = A_{Li+Ele} * \exp exp \left(- \frac{E_{a,Li+Ele}}{RT}\right) * c_{Li+Ele} * \exp exp \left(- \frac{t_{SEI}}{t_{SEI,Ref}}\right) \qquad (2.7)$$

Where:

- $E_{a,Li+Ele}$ is the activation energy

- A_{Li+Ele} is the pre-exponential factor

- $t_{SEI,Ref}$ is the reference thickness

- t_{SEI} is the reference thickness of the SEI layer

Because the concentration of SEI is proportional to its average thickness, eq. 3 can be transformed into eq. 4 [87]

$$\frac{dc_{Li+Ele}}{dt} = A_{Li+Ele} * \exp exp \left(- \frac{E_{a,Li+Ele}}{RT}\right) * c_{Li+Ele} * \exp exp \left(- \frac{c_{SEI}}{c_{SEI,Ref}}\right) \qquad (2.8)$$

Where $c_{SEI,Ref}$ is the reference concentration of the SEI.

The balanced response of SEI degradation and regeneration will continue until the graphite structure collapses at a temperature of 250 °C or higher [36].

2.6.5.3. The reaction at cathode

When the temperature rises to the onset temperature of the cathode decomposition, exothermic reactions occur at the cathode [36]. The most used materials of a commercial lithium-ion battery are LCO, LFP, NCM, and LMO [36]. In our electrolyte characterization, the half-cell has cathode LFP material. As a result, the breakdown of LiFePO4 in the presence of an electrolyte is being explored.

In comparison to other cathode materials, the LFP cathode has high thermal stability [36]. The strong P=O covalent bond of (PO4)3- octahedral structure is one of the reasons for the outstanding thermal properties of LFP. Jiang and Dahn [52] compared the thermal stability of NMC, LCO, and LFP cathode materials using an Accelerating Rate Calorimeter (ARC). The onset temperature for the LFP decomposition was around 310 °C [52].

3 MATERIALS

3.1. Silane Boron-Nitride

Hexagonal boron nitride (h-BN) is a layered material consisting of two-dimensional, atomically thin hexagonal layers [53]. Some characteristic properties of hexagonal boron nitride are:

- o Chemical inertness
- o Non-toxicity
- o High thermal conductivity
- o Low thermal expansion
- o High electrical resistance
- o Low dielectric constant
- o Good thermal shock resistance

BN has been used as filler in polymeric composite to improve thermal, mechanical, and other properties [54]. In the field of energy storage devices, the use of this filler is mostly related to thermal improvement of the separator and electrolyte performances. The polymer separator and electrolyte with improved thermal conductivity have been employed in Li-ion batteries to promote heat dissipation and reduce thermal stress in batteries. The properties of the filler are listed in Table I.

TABLE I. PROPERTIE FOR BORON-NITRIDE FROM LITERATURE

BN	Density	CTE	Particle diameter	Particle length	Thermal conductivity
	2.27 [g/m3]	4.3 [ppm/°C]	4-5 [um]	-	29 [W/m K] @ 30°C

3.2. NMP

N-Methyl-2-pyrrolidone (NMP) is an organic compound consisting of 5- membered lactam.

Because of its non volatility and ability to dissolve a wide range of compounds, it is utilized as a solvent in the petrochemical and plastics industries. NMP is used to dissolve a wide range of polymers due to its high solvent qualities. The low enthalpy of mixing allows nanotubes and nanosheets to be dispersed at high concentration [55]. For this reason, there is a renewed interest in NMP for 2D materials beyond graphene, such as Silane Boron-Nitride. These layered materials require solvents which enable exfoliation from the bulk powder and stabilisation.

Some of NMP properties are listed:

o   It is highly polar and miscible with most organic solvents

o   It mixes well with water in all proportions

o   It has a high flash point when compared to similar solvents

o   It has a high boiling point, a low freezing point, and is easy to handle

o   It is chemically and thermally stable, and is non-corrosive

o

TABLE II. PROPERTIES FOR NMP FROM LITERATURE

Molecular weight	Viscosity	Boiling point	Freezing point	Flash point
99.14 [g*mol^{-1}]	1.89 [mPa*s]	204 [°C]	-23 [°C]	99 [°C]

[56]

3.3. PVDF

Polyvinylidene fluoride is a semi-crystalline highly non-reactive thermoplastic fluoropolymer produced by the polymerization of vinylidene difluoride. Due to its remarkable qualities such as high thermal stability, good chemical resistance, and membrane generation properties, it has been one of the most studied and used polymer-based electrolytes for Li-ion batteries [57]. It has been revealed having a relatively high ionic conductivity and ability to solvate the Li salts with the ether oxygens present along its chains [58].

TABLE III. PROPERTIES FOR PVDF FROM LITERATURE

Molecular wight	Glass transition temperature	Melting point
64.03 [g*mol^{-1}]	-35 °C	178 °C

3.4. LiTFSI

Bis(trifluoromethanesulfonyl)imide, most commonly known as LiTFSI, is a hydrophilic salt. It is a low-lattice energy salt, thus enhancing the dissolution in the polymer. Frequently LiTFSI is used as a lithium-ion source in electrolytes for Li-ion batteries. With its large but light anion, it is possible to produce an amorphous polymer electrolyte. During the years, LiTFSI has obtained great attention from the scientific community as one of the possible substitutes of the widely used LiPF$_6$. Most of the safety issues, concerning the electrolytes, are related to the use of organic carbonates as solvent and LiPF$_6$ as lithium salt [59]. LiPF$_6$ does not offer the best performance in terms of ion mobility and does not present any outstanding characteristic, but it is characterized by a branch of well-balanced properties [59]. LiPF$_6$ suffers from major safety drawbacks:

o   Thermal instability at elevated temperatures

o Decomposition into gaseous PF_5 and LiF

o Hydrolysis, resulting in the formation of HF

However, it has the significant benefit of passivating metallic aluminum by producing a screening layer of AlF_3 and AlO_xF_y that resists oxidative dissolution of aluminum at high anodic potentials [60]. The thermal stability of LiTFSI is one of the most important features of the salt, with a very high dissociation temperature of 360°C [61]. Other relevant properties of this salt are the chemical stability and good electrochemical properties. For these reasons, LiTFSI seems to be a key material for the next generation of lithium-ion batteries.

3.5. Emim-TFSI

1-Ethyl-3-Methylimidazolium Bis (Trifluoromethyl sulfonyl)imide is a common ionic liquid used in organic synthesis and the chemical industry as a solvent [62]. It has been chosen because of its TFSI- anion that promotes amorphicity and plasticizes the polymer [63].

TABLE IV. PROPERTIES FOR EMIM-TFSI FROM LITERATURE

Viscosity	Density	Ionic Conductivity	Electrochemical Window
68.5 [cP] @ 25°C	1.49 [g cm^{-3}] @ 25°C	3.18 [mS cm^{-1}] @ 25°C	4.4 [V]

4 EXPERIMENTAL SECTION

4.1. Chemical Exfoliation of S-BN

The first step in order to prepare the electrolyte ink was the chemical exfoliation of the Silane Boron-Nitride additive. A portion of Silane Boron-Nitride powder was initially immersed in the quantities of 25 mg into 3 ml of N-Methyl-2-pyrrolidone. After that, the sample was sonicated in a 500W FB505 Sonic Dismembrator Fisher Scientific. Timer, pulse, and amplitude were set for our experiment. The sample was sonicated for 9 hours, one second on, two seconds off with an amplitude of 30%.

FIGURE 11. 500W FB505 SONIC DISMEMBRATOR FISHER SCIENTIFIC CONTROL SYSTEM

This technique is one of the most common procedures to exfoliate nanosheets. Although this method is due to the power of sonication, the BN is peeled off, and the plate is broken as well. This creates the disadvantage in making BNNs with a wide plate shape [64].
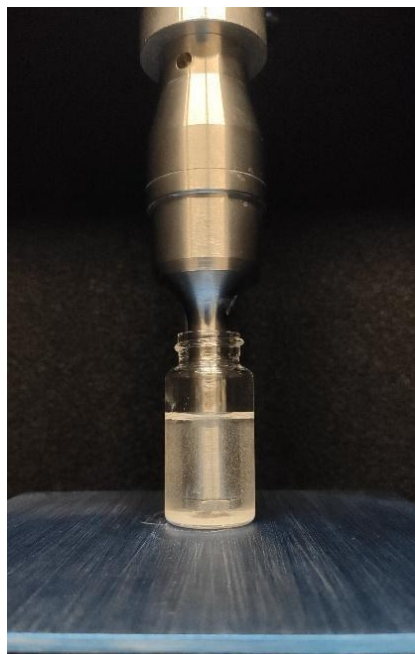
31

FIGURE 12. 500W FB505 SONIC DISMEMBRATOR FISHER SCIENTIFIC DURING SAMPLE SONICATION

4.2. Electrolyte Ink preparation

Once completed the chemical exfoliation, 500 mg Poly(vinylidene fluoride-co-hexa-fluoropropylene) average Mw 400,000 powder (Sigma-Aldrich) was added to the sonicated sample and stirred for 14 hours at room temperature and 450 rpm. At this point, lithium salt and ionic liquid were added to the slurry. 500 mg of 1-Ethyl-3-Methylimidazolium Bis (trifluoromethylsulfonyl)imide ionic liquid were first added into the vials and after that, the slurry was put back to stir. During the stirring, 500 mg of lithium salt were added to avoid lump formation in the electrolyte ink. The sample was left stirring at room temperature at 450 rpm. After 2 hours, the temperature was increased to 80°C and stirred for 12 hours. The final electrolyte ink had the right rheological properties to print the electrolyte with a 3D printing machine. Fig. x is a schematic representation of the used synthesis process.
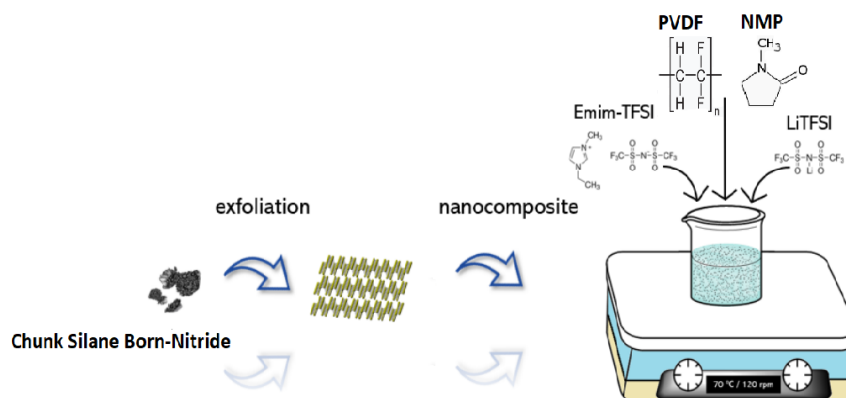
FIGURE 13. SYNTHESIS PROCESS PROCEDURE

4.3. 3D Printing polymer electrolyte

The Nordson EFD EV Series automated dispensing system was utilized to print the gel polymer electrolyte ink 3D printing machine. The automated dispensing system from Nordson EFD sprays fluid onto a workpiece in a pre-programmed pattern.

The DispenseMotion controller, the robot, and the dispensing system components are the primary components of an automated dispensing system. The robot executes a computer program that is created using the DispenseMotion software installed on the DispenseMotion controller. The programs are engineered in order to dispense the fluid in a specific pattern onto a workpiece.
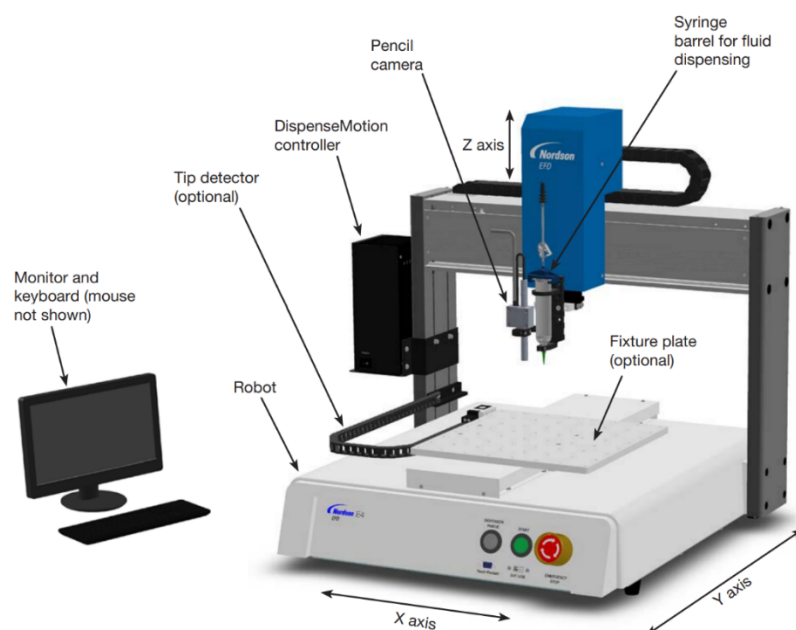
FIGURE 14. NORDSON EFD'S AUTOMATED DISPENSING SYSTEM

During the pre-programmed printing process, the three-axis direction stage moves at a moderate speed to print the desired 3D structure. To adjust the width and thickness of the printed electrolyte, it is possible to adjust dispensing parameters such as air pressure, printing speed, and nozzle size.

4.4. Nordson EFD set up

To print our electrolyte ink, a particular setup for the printer was engineered. In particular, a heating block was installed on the printer to heat up the ink in the syringe, in this way we reduced the viscosity of the electrolyte to facilitate the extrusion through the nozzle of the printer. The heating block was heated by conduction at a temperature of 150 °C. The heating block material was not the only heat source in our set-up, indeed also the fixture plate was heated during the electrolyte printing. The reason why we warmed up the slurry was to reach the

optimum rheologic condition to print, allow the fluid to flow through the nozzle and facilitate the

organic solvent evaporation once the electrolyte was printed.
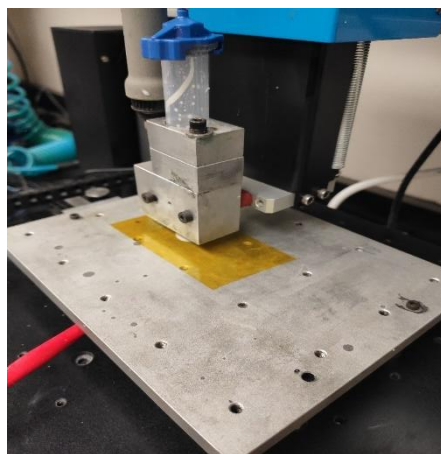

FIGURE 15. NORDSON EFD'S AUTOMATED DISPENSING SYSTEM SETUP

As mentioned, the first step to print the electrolyte was to build the machine setup. At this point,

the machine was turned on with the pump system and the heaters. In the meanwhile, the ink was

transferred from 20 ml vials to a 10 cc Nordson EFD Optimum Barrels.
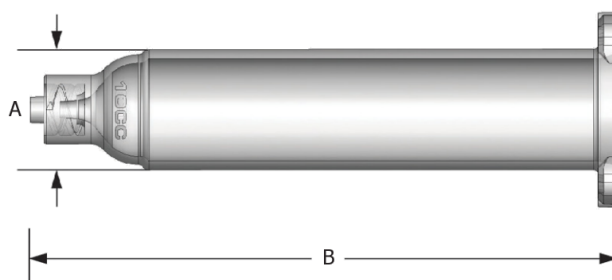
FIGURE 16. 10 CC NORDSON EFD OPTIMUM BARRELS

*T*ABLE *V. 10CC NORDSON EFD OPTIMUM BARRELS DIMENSIONS*

Size	A	B
10 cc	19.1 [mm]	88.9 [mm]

The syringe top was connected to the machine pumping system to provide the necessary pressure to the ink. At the tip of the syringe was connected the nozzle. Two different sizes of general-purpose stainless-steel tips were used during the printing process, 0.41 mm (red) and 0.25mm (blue). The tips provide precise and consistent deposits during the whole process [65].

*F*IGURE *17. G*ENERAL-*PURPOSE STAINLESS-STEEL TIPS*

4.5. Programming

A program is a set of commands stored as a file. There are two types of commands:

- o   A setup commands
- o   Dispense commands

A setup command changes a program-level parameter, such as the Z clearance height or an XYZ location. When a dispense command is linked to an XYZ coordinate, the dispensing system receives an automatic signal to execute the command. Addresses are used to store all commands. When the robot runs a program, it goes through each address one by one, executing the

command contained in each one. The system registers a setup command if it appears in an address. If an address includes a dispense command, the robot moves the X, Y, and Z axes to the place specified in the instruction before executing it.

The following figure shows an overview of the DispenseMotion Software from the Nordson EFD manual.
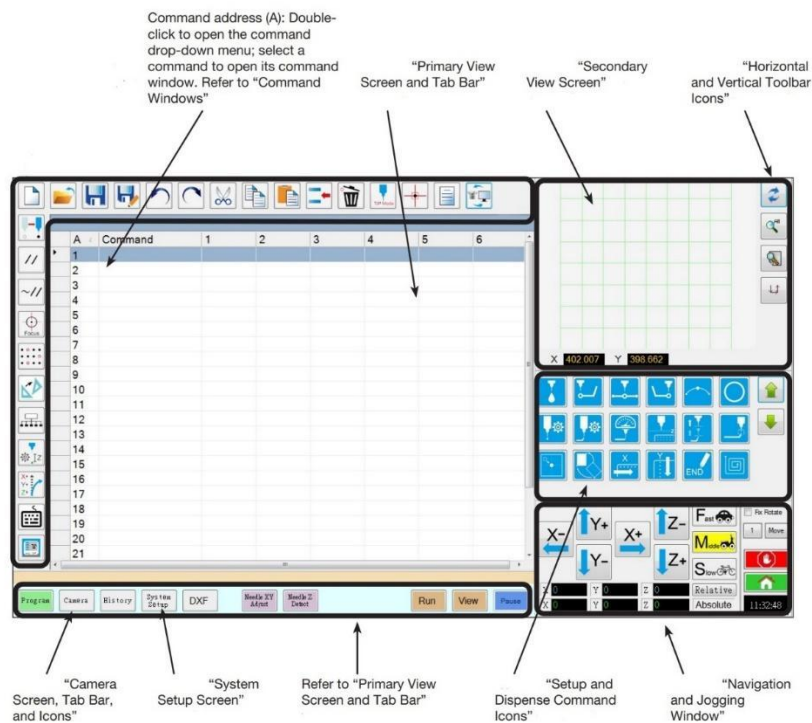

FIGURE 18. DISPENSEMOTION SOFTWARE

To create a program, it is necessary to follow a standard step procedure:

1. Click the green PROGRAM tab

2. Use the navigation icons to move the dispensing tip to the appropriate XYZ point

3. Include a setup or dispense instruction that instructs the robot on how to proceed

4. Repeat steps 2 through 4 until the program is complete

5. Click END PROGRAM to end the program

Once the program is ready, clicking on "View" or "Run" it is possible to test the program and adjust until the program runs correctly.

Two different structures were programmed:

o Full Circle

o Three Parallel Lines

4.5.1. Full Circle

The first path programmed was a full circle. The polymer electrolyte printed with this structure was directly used in the assembly of a coin cell battery.

For this kind of structure, we did not vary the dispensing parameters that were fixed at the beginning.

TABLE VI. DISPENSING PARAMETERS VALUES FOR FULL CIRCLE PRINTING

Line Speed	Air Pressure	Nozzle size
10 [mm/s]	7 [psi]	0.84 [mm]

To create a full circle, the dispensing parameter used was the "circle" command. Once defined the centre of the circle, X and Y position, different diameters were set for each address line. With

this procedure, concentric circles were printed by the robot. The following figure shows the view of the program.
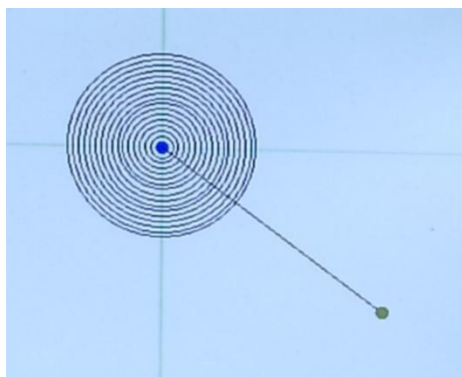
FIGURE 19. CIRCLE PROGRAM VIEW

The green dot represents the "home" position of the robot. Once the program was run, the robot started following the black path. It is important to underline that not all the black lines correspond to ink extrusion, indeed only when the robot was following the circle black line the ink was printed.

An important aspect to take into consideration is the calibration of the Z coordinate. Every new program or set-up change needs a recalibration of the Z coordinate. To perform the calibration, the robot moves from the "home" position to the centre of the circles by double-clicking on the blue dot. At this point, the desired Z coordinate is set manually by jogging the dispensing tip through the Navigation and Jogging Window.

The final printed polymer electrolyte is displayed in figure X.
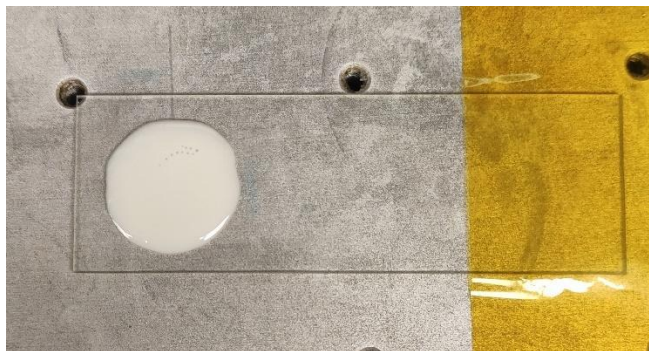
FIGURE 20. CIRCLE PRINTED POLYMER ELECTROLYTE

During the printing process the ink was heated up at 150 °C, while the temperature of the plate was 80°C.

4.5.2. Three Parallel Lines

The three parallel line structure was printed in order to perform an analysis of the relation between the morphology of the final printed structure and the dispensing parameters.

The dispensing parameters of interest were the nozzle speed, the air pressure, and the nozzle size. Three structures with the same geometry were printed. For each sample, two parameters were kept fixed while varying the other one. In this way, it was possible to highlight the different influence of the three parameters on the final printed result.

To create the three parallel lines, the "line" dispensing command was used. In this case, it was necessary to define three different X and Y coordinate positions to start printing the line. Even in this case, the calibration of the Z coordinate was performed manually and for each different set-up. The distance between the lines was 10 mm. The view of the program is displayed in the following picture.
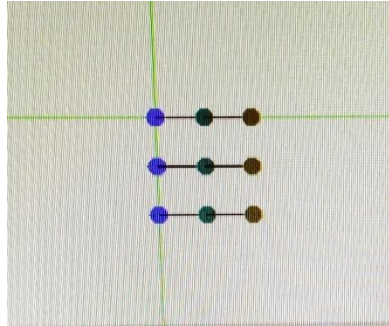
FIGURE 21. THREE LINES PROGRAM VIEW

In order to demonstrate the influence of the dispensing parameters, the ink was printed with the following settings:

o   Influence of air pressure: The printing speed and nozzle sizes were set at 10 mm/s and 0.41 mm, respectively. Three different settings of the air pressure (20, 40, and 60 psi) were used.

o   Influence of printing speed: The air pressure and nozzle sizes were set at 40 psi and 0.41 mm, respectively. Three different settings of printing speeds (5, 10, and 15 mm/s) were used.

o   Influence of nozzle tip size: The air pressure and printing speeds were set at 60 psi and 10 mm/s, respectively. Two different settings of the nozzle size (0.25 and 0.41 mm) were used.

During the printing process, the ink was heated up at 150 °C, while the temperature of the plate was 60°C.

FIGURE 22. THREE LINES PRINTED ELECTROLYTE

4.6. Dispensing parameters analysis

The dispensing parameters analysis was performed on the three lines structure printed with the Nordson EFD 3D printing machine. The analysis was performed to understand the influence of the dispensing parameters on the final shape of the printed el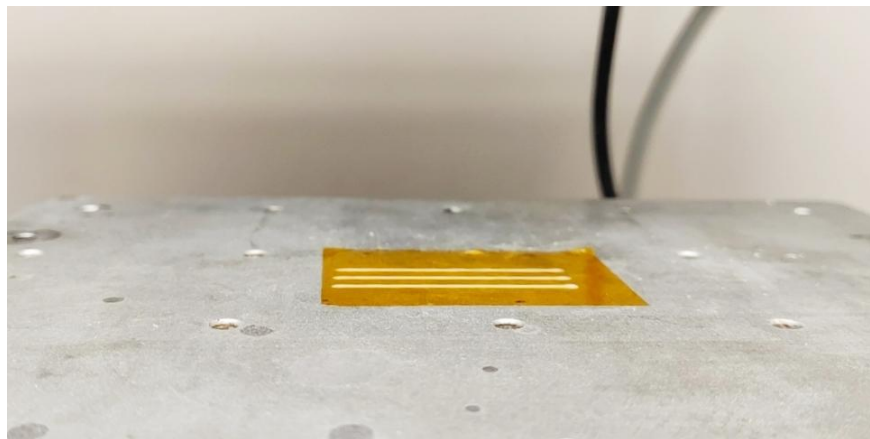ectrolyte. This kind of analysis becomes very important if the focus is the shift to the commercialization of 3D printed batteries.

The advantages in microelectromechanical systems, sensing technologies, and low-power wireless communications drove the research efforts in developing micro-batteries. High precision and low tolerance are required for this kind of application. For these reasons, it is crucial to understand the relation between air pressure, nozzle speed, and nozzle size on the final printed product. From the point of view of the manufacturer, the optimum in terms of time and energy consumption efficiency is the final goal. For instance, if the same product characteristics can be reached with a higher nozzle speed, it is possible to fabricate more units in less time, keeping the same product quality standard.

The thickness and the width of each sample were measured with a digital caliper. The 40 mm line was divided into 10 parts that corresponded to 10 thickness and width measurements. This

technique was used in order to understand the different distribution of the ink during line printing.

The device used to perform the measurements for this test is a Neiko stainless hardened digital caliper. The range of measurement of the instrument is $0 - 150$ mm, with an accuracy of 0.02 mm.

FIGURE 23. NEIKO STAINLESS HARDENED DIGITAL CALIPER

4.7 Li-Ion polymer cell assembly

The cell was assembled as a 2032 MTI coin-type cell in a glove box. The glove box is designed for use in controlled atmospheres, it provides a leak-tight environment for work with contamination-sensitive materials. Lithium is very reactive with moisture and air and its exposure may affect the cell performances. Two different kinds of coin cells were assembled depending on the test that was performed.

The coin polymer electrolyte previously printed was left in an oven (look for the brand) for 24 h at 80°C. This procedure is necessary to evaporate the organic solvent present in the ink (NMP).

The Li-symmetrical cell was assembled for the overpotential test. Both the anode and the cathode of the cell were made of Li, and the printed gel polymer electrolyte was put between the two electrodes.

For cycling and thermal runaway tests, a half-cell was fabricated. The whole process took place in the glove box. The coin cell fabrication followed a straight procedure:

- o Displace a negative case on a non-conductive surface

- o Add a stainless-steel spring

- o Place a stainless-steel spacer

- o At this point, a LFP cathode was added

- o The gel polymer electrolyte was lean on the LFP

- o A Li foil was used as anode

- o The cell assembly is completed with a positive top casing
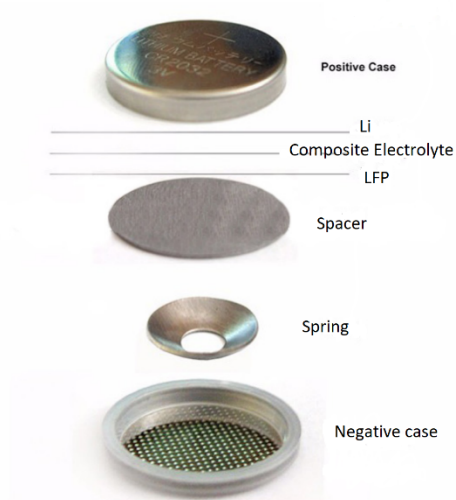
- o The coin cell is ponce to let all the layer stack

FIGURE 24. HALF COIN CELL ASSEMBLY

4.8. Overpotential

To evaluate the operational properties of the 3D printed gel-polymer electrolyte, the overpotential test is performed. The aim of the test is to give information regarding the ease for Li-ions to travel through the electrolyte, but also about the interfacial properties. The interfacial properties describe the contact between the electrolyte and the electrode [66]. Better interfacial properties correspond to a better ability of the electrolyte to cover the electrode surface, with a consequent improvement in Li ions transport.

For this test, a Li-symmetrical cell was used, and different rates are used for a brief amount of time to let the Li ions go from one side to the other. In the ideal case, lithium stripping and plating occur, letting the Li intercalates and de-intercalates within/from the electrodes:

$$Li^+ + e^- \longrightarrow Li$$

Preferably, the curve result of the overpotential test should be a line. That means that the resistance faced by the Li ions is negligible. Of course, in the real world that is not possible, and the final result will not be a line. The overpotential can be expressed as:

$\Delta v = \Delta vb + \Delta vint = Rb \cdot I + Rint \cdot I$

where:

- o Δvb is the overpotential due to the bulk electrolyte [V]
- o $\Delta vint$ is the overpotential due to the electrolyte/electrode interface [V]
- o Rb is the resistance due to the bulk electrolyte [Ω]
- o $Rint$ is the resistance due to the electrolyte/electrode interface [Ω]
- o I is the used current [A]

The overpotential tends to increase over time, due to the many phenomena such as cations trapping, an increase of SEI thickness, electrode degradation, etc. [67].

BTS-4008-5V10mA neware battery cycler was used for the measurements. The coin cell was tested for 500 hours at 0.05 mA cm-2 with a full one-hour cycle (30 minutes charge – 30 minutes discharge).

4.9. Charge-discharge cycling

The charge-discharge cycling is an important test that shows if the gel-polymer-electrolyte can effectively work within a battery. During this test, the coin cell is tested at different current intensities, in this way it is possible to understand how the electrolyte will perform at a certain rate. From the electrolyte point of view, not all the current intensities are possible. While a liquid electrolyte can deal with very high C-rates, a gel- or solid-state electrolyte is limited by its own chemical and physical characteristics. Furthermore, the evolution in time of the extracted capacity from the cathode is analysed. This is a fundamental analysis since the user finally wants to buy and use a durable and reliable device. For these reasons, the three samples were cycled at different C-rates. The used cut-in and cut-off voltage are imposed by the typology of the cathode; for LFP, 2.5 and 4.2 V are usually selected. Voltage control with very small tolerances is necessary to make the Li-ion battery last longer. Fatal reactions can occur at high voltages which can compromise safety and battery cyclability. When a rechargeable battery is charged, the anode overcomes a reduction taking electrons and receives Li cations, which intercalate in its structure. At the same time, the cathode oxidizes.

Traditionally, the C-rate was introduced by battery manufacturers and users, and expressed the current needed to charge or discharge a cell in a specific amount of time:

$C - rate = C \cdot g \ 1000 \cdot h$

where:

- o C is the specific capacity of the cathode [mAh/g]

- o g is the weight of the present active material [mg]

- o 1000 is a unit conversion [g/mg]

- o h is the amount of time [h]

This means that, if one would like to cycle the battery at the rate of C/10, it is expected to have a 10-hour charge and discharge, respectively.

Three LFP/Li coin cells were tested with BTS-4008-5V10mA Neware battery cycler; different C-rates were used. More in detail, 0.5C, 0.2C, and 0.1C were run at 25°C.

The coulombic efficiency (CE), also called faradaic efficiency or current efficiency, can be defined by this test. It describes the charge efficiency by which electrons are transferred in batteries [68]. By definition this quantity is:

$$\eta = \frac{discharge\ capacity}{charge\ capacity}$$

4.10. Electrolyte thermal characterization

As discussed in the previous paragraphs, the thermal runaway is a safety issue that is being the focus of the scientific community research activity. The reduction of the hazard caused by thermal runaway can be achieved in different ways, depending on the thermal runaway process stage.
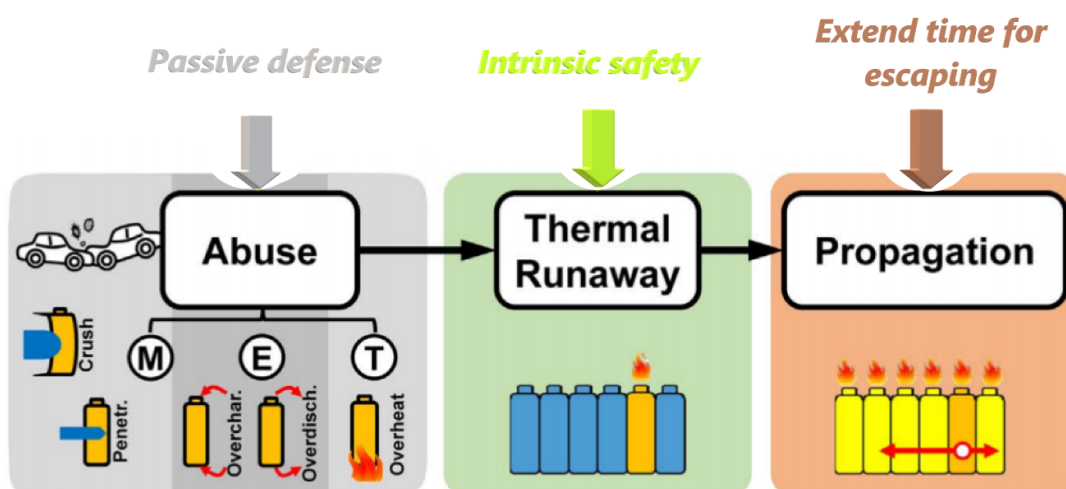
FIGURE 25. THERMAL RUNAWAY PROCESS STAGE

Figure n displays the three different stages of the thermal runaway process and the respective three "reduction of the hazard" solutions.

In this project the intrinsic safety, especially the anti-thermal runaway properties, of the cell was improved by material modification.

Because the thermal stability of the system is largely dependent on the thermal safety of the entire cell, material modification can be done on the cathode, anode, separator, and electrolyte.

Innovative and improved electrolyte systems, such as ionic-liquids, polymer electrolytes, and solid electrolytes, have the potential to overturn the entire electrolyte system. As a result, the electrolyte used in this study was a 3D printed gel-polymer electrolyte.

During the polymer electrolyte synthesis process, a Silane Boron-Nitride ceramic filler was added to the electrolyte slurry with the purpose of reaching the optimum ink viscosity and increasing the thermal properties of the electrolyte.

Once printed on the electrolyte, the half coin cell with LFP cathode and gel-polymer electrolyte was thermally tested and, to define the thermal performance of the novel electrolyte, a comparison between the performance of the polymer and liquid electrolyte was conducted.

The data acquisition was performed with a thermal imaging camera. The infrared camera used is a HT19 Thermal Imager, that integrates surface temperature measurement and real-time thermal image.

FIGURE 26. THERMAL CAMERA

The camera can detect a temperature range varying from -20 °C to 300 °C with a resolution of 320x240.

During the experiment, the coin cell was heated up on a hot plate to define the thermal distribution of the coin cell surface and the evolution in time of the temperature. Different plate temperatures were set to 60 °C, 80 °C, 100 °C.

One of the problems to solve with the experimental setup was the reflection of the coin cell surface , in fact the surface of the coin cell had a high reflectivity, and the camera was not able to properly detect the temperature of the surface. To avoid the reflection problem, the coin cell was coated with a carbon tape. The carbon tape was chosen because of its good thermal conductivity property and low reflection coefficient.

FIGURE 27. COIN CELL CARBON TAPE COATING

The carbon tape was also used on the hot plate to create a homogeneous temperature distribution.
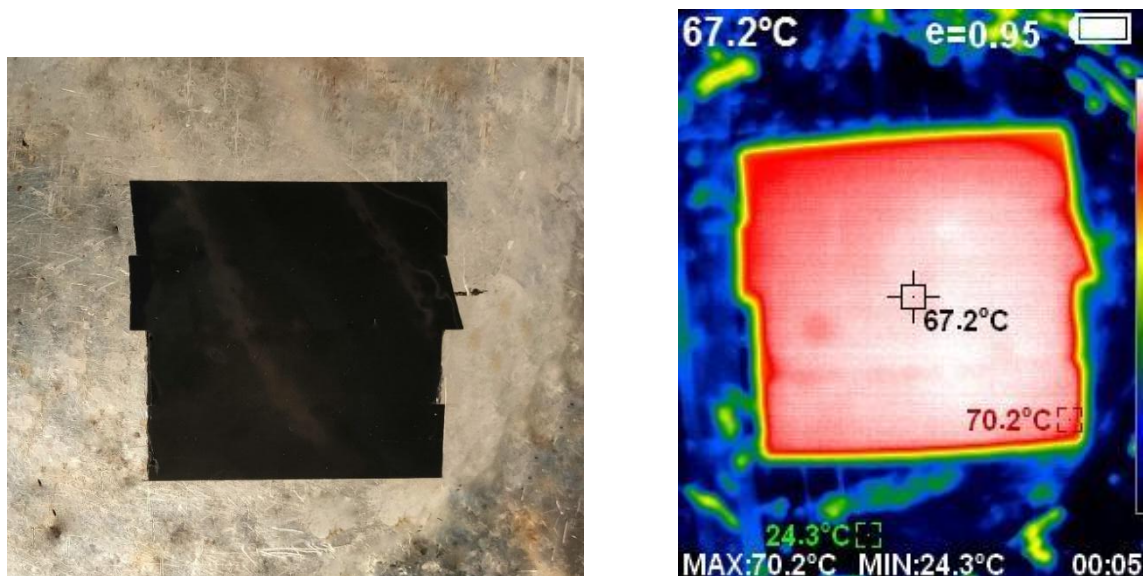
FIGURE 28. THERMAL IMAGE OF THE HOT PLATE AT $60°C$

Once built the setup of the experiment, the coin cell was collocated in the middle of the hot plate and the temperature evolution was recorded.

5 RESULTS AND DISCUSSION

5.1. Overpotential results

The overpotential test was conducted on a Li/Li cell with the printed electrolyte. The overpotential is expected to increase over time because of the spontaneous increase of resistance, due to cations trapping, an increase of SEI thickness, electrode degradation, etc. [67]. The increase is more aggressive at higher currents [69], because the cell is more stressed than for lower currents. The cell was tested for 500 cycles, each cycle was characterized by 30 minutes of charge and 30 minutes of discharge, as displayed in figure 25. For the printed electrolyte test, a low-rate current was investigated in order to investigate the performance of the electrolyte in no-hostile conditions. As shown in figure 25, for a 0.05 mAcm^{-2} and room temperature, 5the overpotential range is almost constant for the whole test time. This means that the electrolyte does not have a high degradation rate, which is reflected in a good battery cyclability.
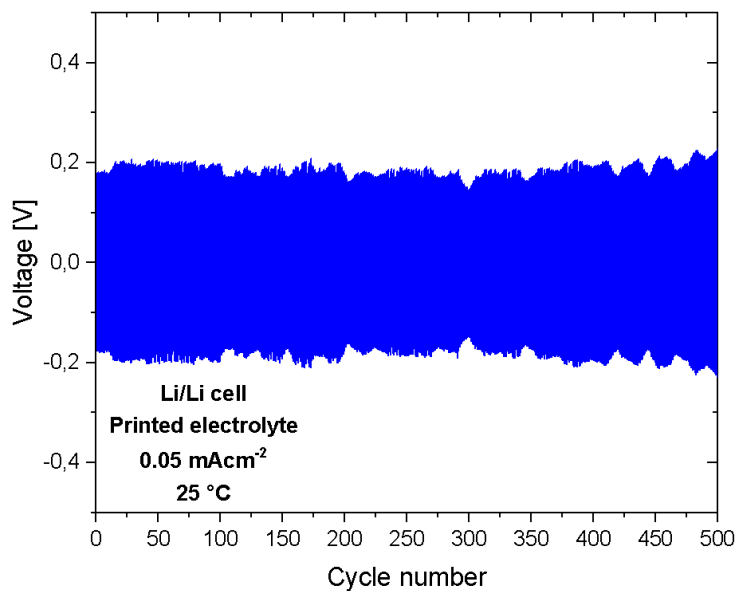

FIGURE 29. OVERPOTENTIAL FOR 3D PRINTED ELECTROLYTE

The overpotential results point out that Li+ cations do not find high resistance to reach the electrodes using a printed electrolyte with nanoscale additive, so the performances of the printed electrolyte are promising for future application. A better understanding of the results can be pointed out by further studies such as a simulation of the electrolyte/electrode interface or SEM analysis of the battery components.

5.2. Charge and discharge profile results

Before starting the discussion about the charge and discharge test, it is valuable to underline the difference between practical and theoretical capacity [mAh/cm^2]. In fact, the practical capacity is always smaller than the theoretical one because the cell does not operate on a very wide voltage window and not all the lithium cations can be extracted from the lattice of the host material within that voltage window.

In this project, four half coin cells Li/LFP were charged and discharged at three different C-rates. The voltage vs time and the voltage vs capacity have the same behavior since the capacity is monotonically dependent on time. When charging the capacity increases up to 4.2 V, while discharging, it decreases down to 2.5 V. The data collected for the first charge/discharge cycle in the test are shown in the following graphs.
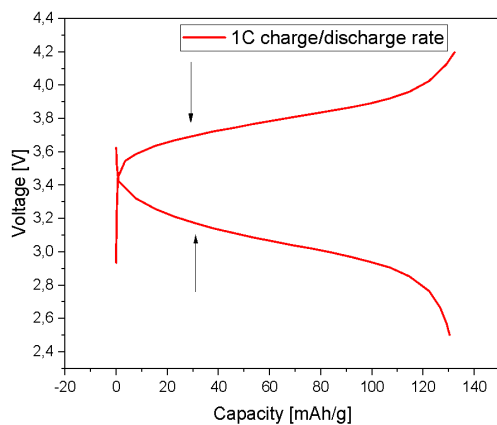
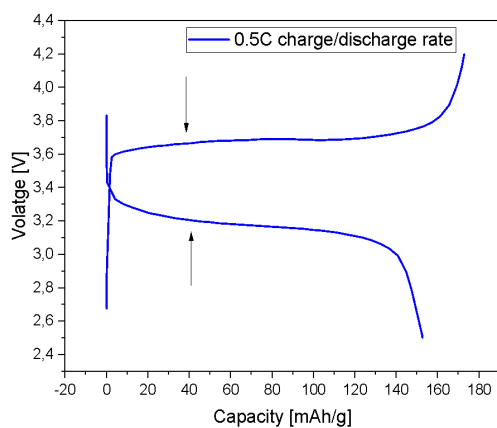*FIGURE 30. CHARGE AND DISCHARGE PROFILE OF THE PRINTED ELECTROLYTE AT 1C*

FIGURE 31. CHARGE AND DISCHARGE PROFILE OF THE PRINTED ELECTROLYTE AT 0.5C
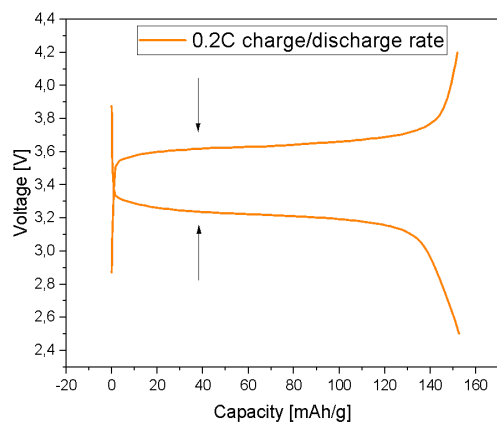
FIGURE 32. CHARGE AND DISCHARGE PROFILE OF THE PRINTED ELECTROLYTE AT 0.2C
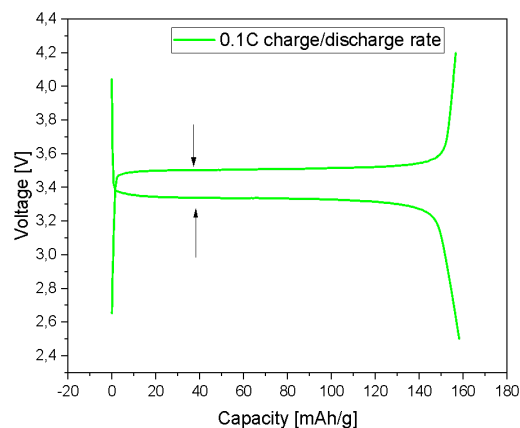

FIGURE 33. CHARGE AND DISCHARGE PROFILE OF THE PRINTED ELECTROLYTE AT 0.1C

The C-rate is a measurement of how quickly a battery charges or discharges. The theoretical current draw required to deliver the battery's nominal rated capacity in one hour is divided by the current flowing through the battery. To investigate the behavior of the printed electrolyte, 0.5C, 0.2C, 0.1C, and 1C were implemented for the test. The different C-rates correspond respectively to 1 hours, 2 hours, 5 hours, and 10 hour charging-discharging process.

As it is possible to notice from the four graphs, the behavior of the battery is different for the different current intensities. The first topic of the analysis is overpotential. The difference in voltage between the charging and discharging process tends to decrease at the lowest C-rate. This can be explained by an inevitable supplementary resistance collected over time by the electrolyte. On the other hand, high currents stress the cell more with consequent degradation of the cell performances.

The other important aspect of the test was the evaluation of the capacity of the cell. The mass of active material in the battery determines the battery capacity [Ah], which is a measure of the charge stored by the battery. Under particular conditions, the battery capacity represents the greatest amount of energy that can be retrieved from the battery. The rated battery capacity is influenced by the charging/discharging speeds. The quantity of energy that can be recovered from the battery is lowered when the battery is depleted quickly, and the battery capacity is diminished. One of the causes is that the reaction's components do not always have enough time to shift to their required places. Only a small portion of the total reactants are transformed to other forms, reducing the amount of energy available [70].

On the other hand, if the battery is charged/discharged slowly and with a low current, more energy is stored/extracted and the battery capacity is increased.

The test findings reflect the previously reported behavior. The capacity of the cell at a C-rate of 1 is around 130 mAhcm-2, which is lower than the other C-rates.

It is also worthy to underline how the battery capacity decreases after the first cycle. A good-performing battery should have a low degradation rate during the time, and the behavior of the printed electrolyte is promising for commercial application. The following graph displays the degradation over the time of the battery. The battery is charged/discharged at 0.2C rate and 150 cycles are plotted. As expected the capacity of the cell decreases after the first cycle although the battery shows good performances after the first 150 cycles.
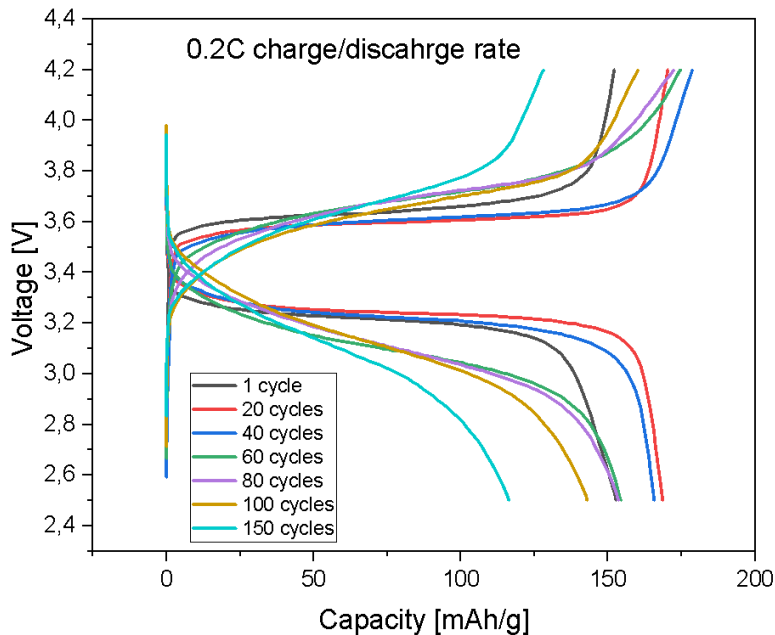
FIGURE 34. CHARGE AND DISCHARGE PROFILE OF THE PRINTED ELECTROLYTE AT 0.2C FOR 150 CYCLES

The amount of energy that can be collected from a battery is likewise affected by its temperature [70]. The battery capacity is often higher at higher temperatures than at lower temperatures. Intentionally raising battery temperature, on the other hand, is not an efficient way to improve battery capacity without also lowering battery longevity.

It is valuable to underline how the printed electrolyte did not fail during the charging/discharging test at different C-rates, exhibiting interesting electrochemical performances.

5.3. Dispensing parameters analysis

The dispensing parameters analysis was conducted to define a correlation between the air pressure, nozzle speed, and nozzle size dispensing parameters and the morphology of the final

printed product. As mentioned previously, one of the many features of the printed batteries is the possibility of fabrication of functional systems with batteries already integrated into devices. However, high accuracy is required during the extrusion of the ink to achieve the desired results.

5.3.1. Air pressure

The analysis of the influence of the value of the air pressure on the printed structure was conducted keeping constant the nozzle size and the nozzle speed. The width and the height of three straight lines were measured and the result is displayed in the following graphs.
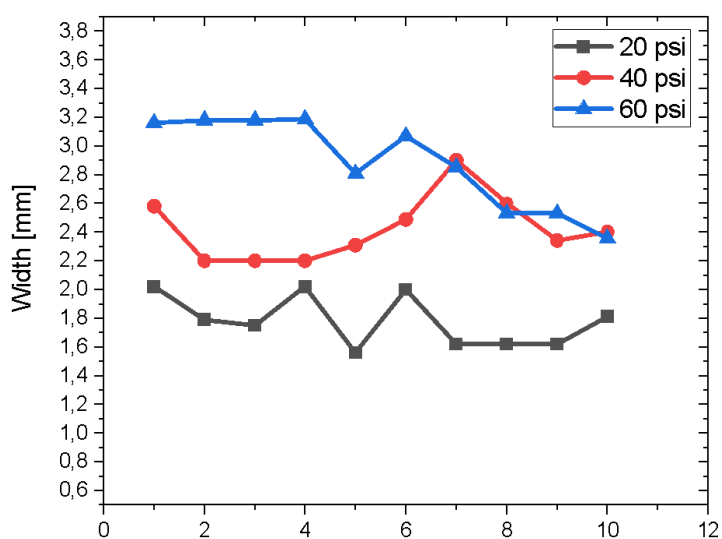

FIGURE 35. WIDTH MEASUREMENTS OF THE SAMPLE PRINTED AT CONSTANT NOZZLE SPEED AND SIZE, 10 MM/S AND 0.41 MM RESPECTIVELY
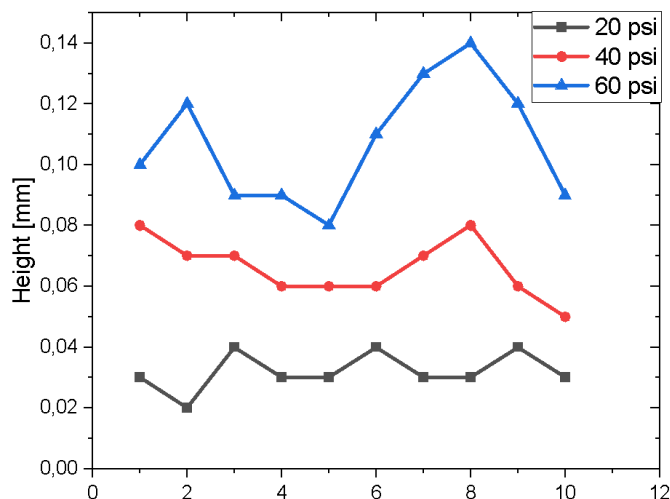
FIGURE 36. HEIGHT MEASUREMENTS OF THE SAMPLE PRINTED AT CONSTANT NOZZLE SPEED AND SIZE, 10 MM/S AND 0.41 MM RESPECTIVELY

As it is possible to understand from the graphs, a higher-pressure value is related to major ink extrusion and in consequence higher and wider printed structure. It is worthy to underline how the height of the printed structure is more visible than the width. In both graphs, the distribution of the ink at lower pressure is more uniform and can be correlated to a higher precision during the printing process. The height of the printed electrolyte is unequal, highlighting less accuracy during the printing.

In general, the set of the air pressure value for 3D printing battery solution should take into consideration the level of accuracy that is required to manufacture the battery.

5.3.2. Nozzle speed

The nozzle speed is the speed at which the robot arm moves during the printing process. The nozzle speed was modified during the program set-up and three different speeds were analyzed.

The study of the speed influence on the printed electrolyte is interesting from the point of view of the manufacturing process.

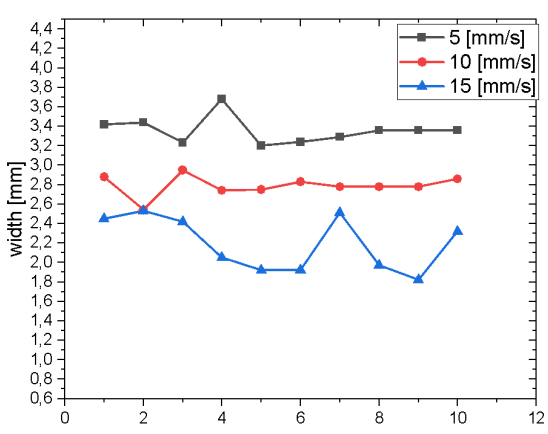The graphs describe the distribution of the ink at fixed air pressure and nozzle size.

FIGURE 37. WIDTH MEASUREMENTS OF THE SAMPLE PRINTED AT CONSTANT AIR PRESSURE AND NOZZLE SIZE, 40 PSI AND 0.41 MM RESPECTIVELY
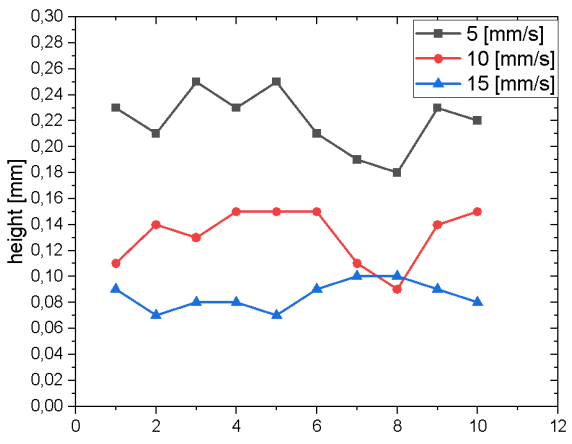

FIGURE 38. HEIGHT MEASUREMENTS OF THE SAMPLE PRINTED AT CONSTANT AIR PRESSURE AND NOZZLE SIZE, 40 PSI AND 0.41 MM RESPECTIVELY

At elevated speed, the robot machine deposits less ink, and this is reflected in the geometry of the printed structure. For high-speed rate, the width and height of the sample are limited, while for low-rate velocity (10 mm/s, 5 mm/s) the increment in dimensions of the sample is around 36% for the height and around 63% for the width.

In this case, in the three experiments, the distribution of the ink is relatively regular during the whole printing process.

5.3.3. Nozzle size

The nozzle size influence on the printed electrolyte was conducted keeping constant the air pressure and the printing speed. The analysis aims to understand the distribution of the ink during the printing process. Understandably, the dimension of the printed structure would be different because of the different sizes of the nozzle, but it is interesting to study the distribution of the ink at different printing scales.
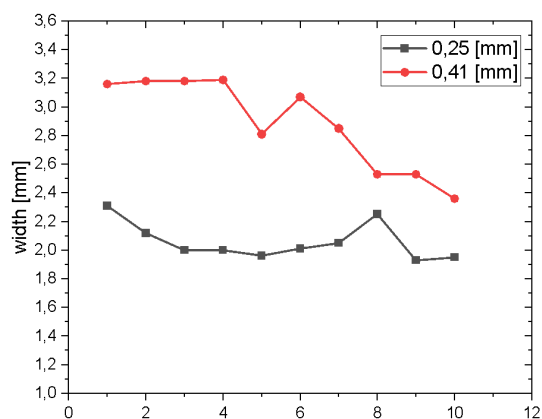
FIGURE 39. WIDTH MEASUREMENTS OF THE SAMPLE PRINTED AT CONSTANT NOZZLE SPEED AND AIR PRESSURE, 10 MM/S AND 60 PSI RESPECTIVELY
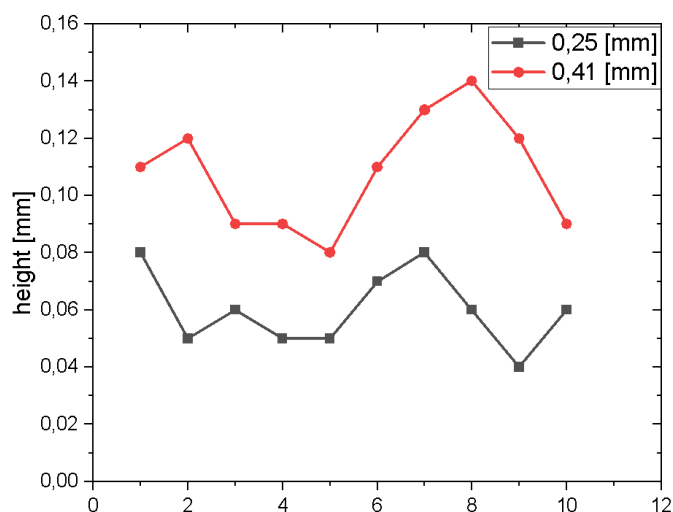
FIGURE 40. HEIGHT MEASUREMENTS OF THE SAMPLE PRINTED AT CONSTANT NOZZLE SPEED AND AIR PRESSURE, 10 MM/S AND 60 PSI RESPECTIVELY

The two graphs show the width and the height of two samples printed with a 0.25 mm and 0.41 mm nozzle diameter. It is interesting to underline how for a smaller diameter size, the distribution of the ink is more homogeneous, especially for the width of the sample.

The result shows that the ink composition implemented in this project, can be printed with different dispensing parameters set-up, and still maintaining excellent printability properties.

5.4. Thermal characterization results

The aim of the test was to understand the behavior of the coin cell under thermal abuse conditions. The distribution of the heat and the evolution of the temperature over 180 seconds were analyzed. Three different plate temperatures were set: 60, 80, 120 °C.
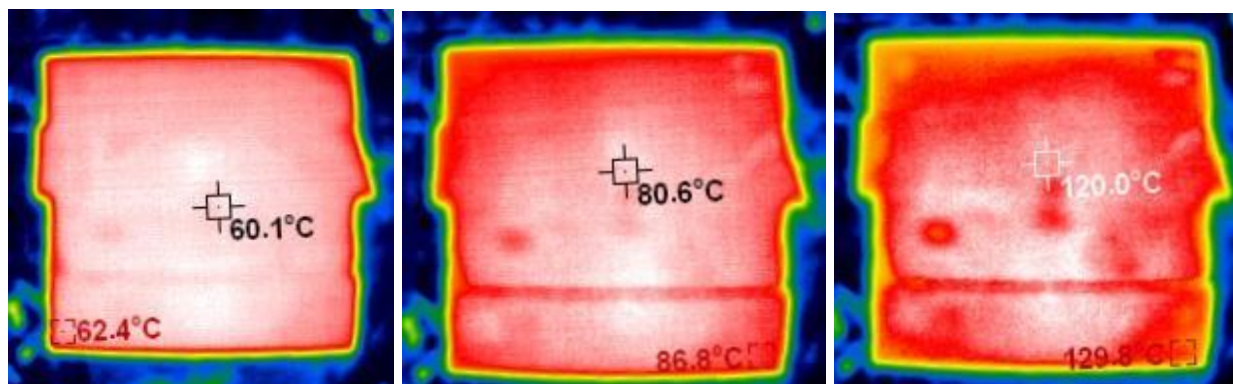
FIGURE 41. HOT PLATE AT DIFFERENT TEMPERATURE

The coin cell with h-BN polymer electrolyte, was collocated in the middle of the hot plate square. Images at different times, during the experiment, show the distribution and the evolution of the temperature in the coin cell.
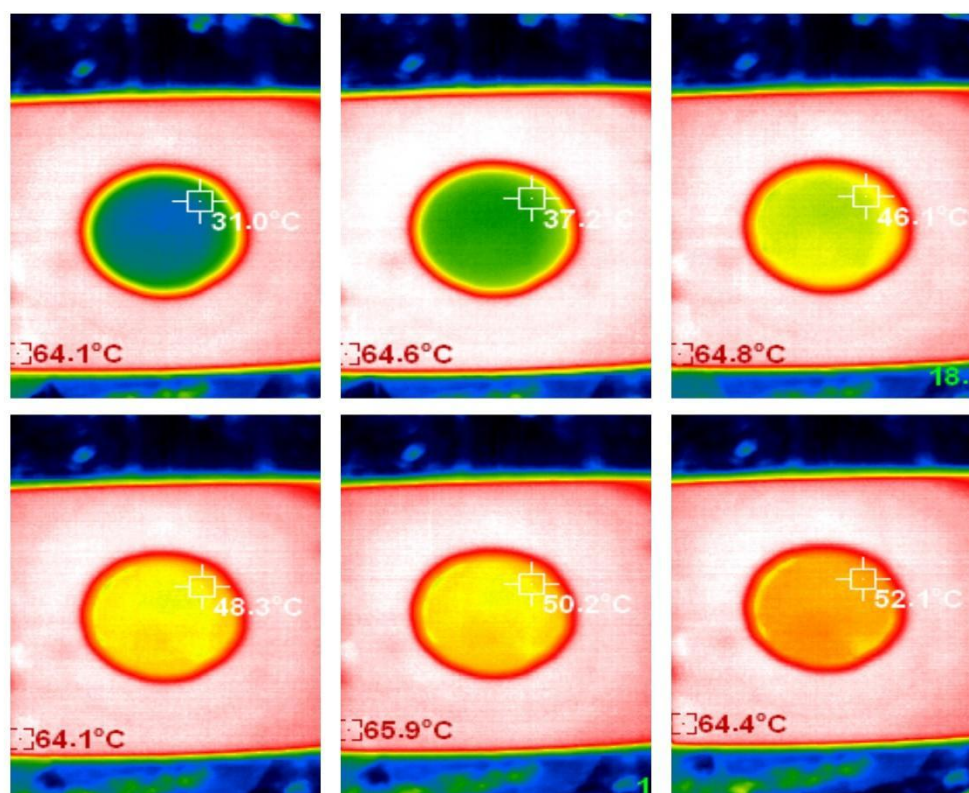
FIGURE 42. EVOLUTION OF THE TEMPERATURE OF A COIN CELL WITH POLYMER ELECTROLYTE ON A HOT PLATE AT 60°C

The same analysis was conducted for the hot plate at 80°C and 120 °C (see Appendix, fig. 41, 42).

As displayed in the previous figure, it is possible to visualize that the temperature distribution is homogeneously distributed on the coin cell surface, and no local hot spots are present. This is a significant result that shows the good behavior of the system under thermal stress conditions.

The temperature evolution was monitored for 180 seconds, and the data are plotted in the following graph.
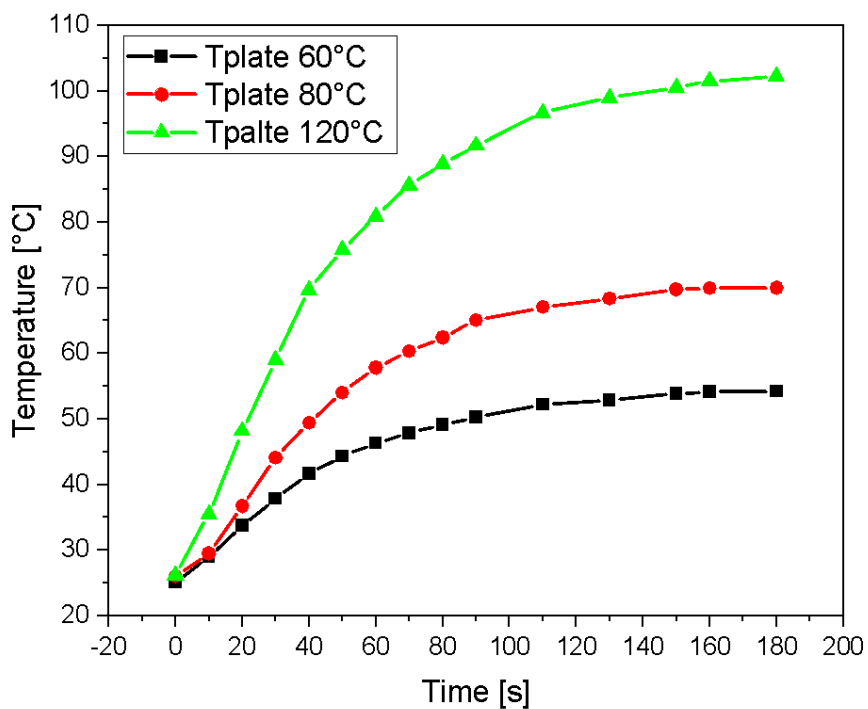
FIGURE 43. TEMPERATURE EVOLUTION FOR A POLYMER ELECTROLYTE COIN CELL

At this point, a comparison with a liquid electrolyte was conducted. The evolution of the temperature for the different coin cells on a hot plate at 120 °C was studied, and it reveals that the presence of the h-BN modified polymer electrolyte effectively improve the thermal properties of the cell, in fact, the temperature of the h-BN cell is lower than the temperature of the cell with liquid electrolyte.
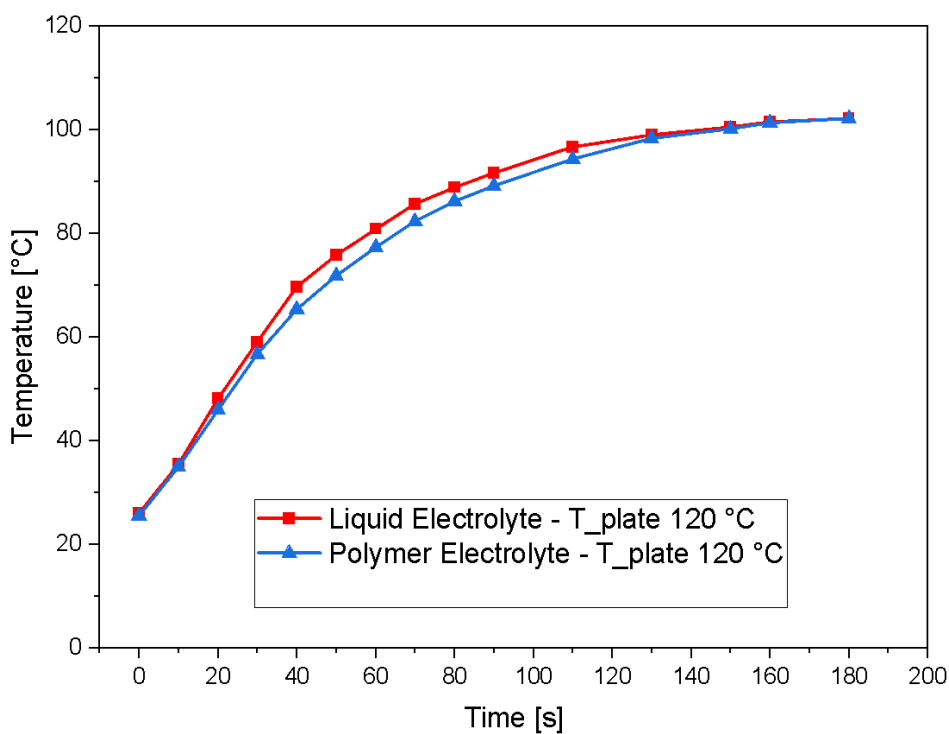
FIGURE 44. LIQUID VS POLYMER ELECTROLYTE TEMPERATURE EVOLUTION

From the graph it is possible to see how the coin cell with polymer electrolyte keeps a lower temperature in the range of 30 to 140 seconds, which means that the temperature increase within the coin cell is limited by the h-BN polymer electrolyte.

The final consideration about the thermal analysis is that the h-BN filler has a good influence on the thermal properties of the polymer electrolyte. The temperature is uniformly distributed, and

no dangerous hotspots are present over the cell surface, which demonstrate the good thermal performance of the electrolyte.

Other types of thermal test can be conducted to better understand the effective role played by the Silane Boron-Nitride filler.

6 CONCLUSIONS

The main focus of the thesis was on the efforts and problems of developing and optimizing the ink for the electrolyte battery component to meet the requirements of efficiency, stability, and processability.

The thesis demonstrates the possibility of manufacturing battery components with enhanced thermal properties making use of 3D printing technologies. The Silane Boron-Nitride filler was able to modify properly the rheological and thermal properties of the electrolyte ink. Moreover, the printed polymer electrolyte showed interesting electrochemical properties such as overpotential and cyclability.

Further efforts are needed to completely prove all the advantages of Silane Boron-Nitride, however the achieved results are without any doubt promising.
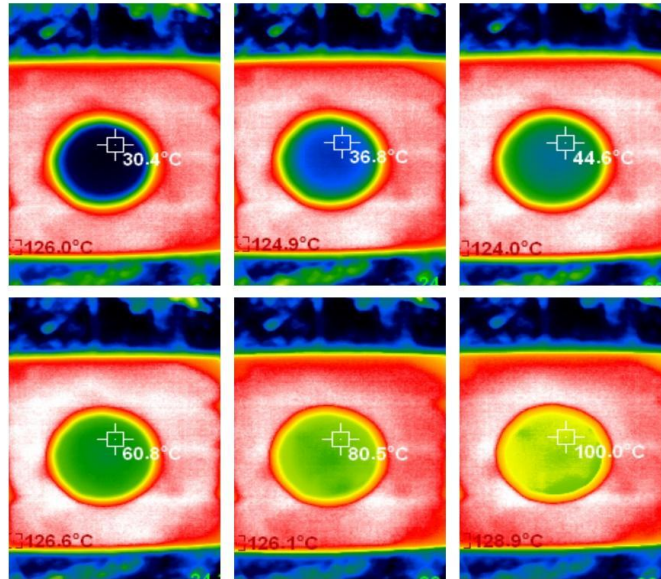
7 APPENDIX

FIGURE 45. EVOLUTION OF THE TEMPERATURE OF A COIN CELL WITH POLYMER ELECTROLYTE ON A HOT PLATE AT 80°C
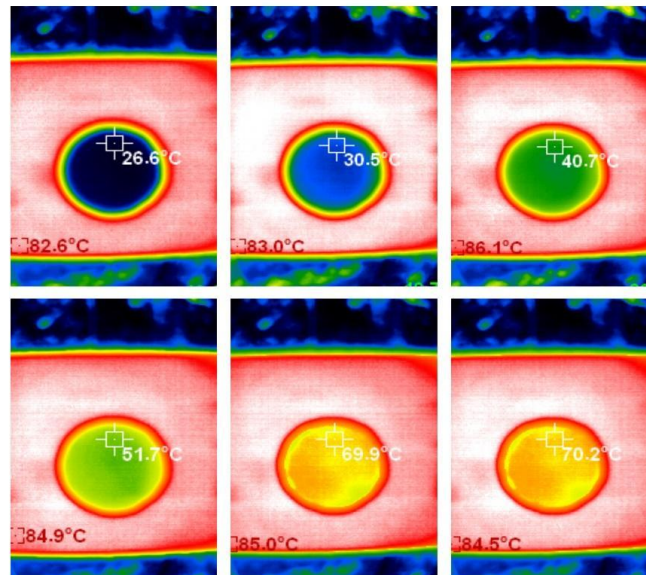

FIGURE 46. EVOLUTION OF THE TEMPERATURE OF A COIN CELL WITH POLYMER ELECTROLYTE ON A HOT PLATE AT 120°C

CITED LITERATURE

[1]   T. Osaka and M. Datta, Eds., *Energy Storage Systems in Electronics*. London: CRC Press, 2000. doi: 10.1201/9781482296891.

[2]   O. M. Toledo, D. Oliveira Filho, and A. S. A. C. Diniz, "Distributed photovoltaic generation and energy storage systems: A review," *Renewable and Sustainable Energy Reviews*, vol. 14, no. 1. Pergamon, pp. 506–511, Jan. 01, 2010. doi: 10.1016/j.rser.2009.08.007.

[3]   H. Chen, T. N. Cong, W. Yang, C. Tan, Y. Li, and Y. Ding, "Progress in electrical energy storage system: A critical review," *Progress in Natural Science*, vol. 19, no. 3. Science Press, pp. 291–312, Mar. 10, 2009. doi: 10.1016/j.pnsc.2008.07.014.

[4]   D. A. J. R. R M Dell, *Understanding Batteries*. Cambridge: Royal Society of Chemistry, 2007. doi: 10.1039/9781847552228.

[5]   J. B. Goodenough and K. S. Park, "The Li-ion rechargeable battery: A perspective," *Journal of the American Chemical Society*, vol. 135, no. 4. pp. 1167–1176, Jan. 30, 2013. doi: 10.1021/ja3091438.

[6]   A. M. Gaikwad, A. C. Arias, and D. A. Steingart, "Recent Progress on Printed Flexible Batteries:Mechanical Challenges,Printing Technologies,and Future Prospects", doi: 10.1002/ente.v3.4/issuetoc.

[7]   M. Park, X. Zhang, M. Chung, G. B. Less, and A. M. Sastry, "A review of conduction phenomena in Li-ion batteries," *Journal of Power Sources*, vol. 195, no. 24. Elsevier, pp. 7904–7929, Dec. 15, 2010. doi: 10.1016/j.jpowsour.2010.06.060.

[8]   A. M. Gaikwad, A. C. Arias, and D. A. Steingart, "Recent Progress on Printed Flexible Batteries:Mechanical Challenges,Printing Technologies,and Future Prospects", doi: 10.1002/ente.v3.4/issuetoc.

[9]   C. Milroy and A. Manthiram, "Printed microelectrodes for scalable, high-areal-capacity lithium-sulfur batteries," *Chemical Communications*, vol. 52, no. 23, pp. 4282–4285, Mar. 2016, doi: 10.1039/c5cc10503j.

CITED LITERATURE (continue)

[10]   M. Cheng *et al.*, "Direct Ink Writing of Polymer Composite Electrolytes with Enhanced Thermal Conductivities," *Advanced Functional Materials*, vol. 31, no. 4, Jan. 2021, doi: 10.1002/adfm.202006683.

[11]   K. H. N. K. Tyler Bartholome, "Lithium Ion Batteries, What are lithium ion batteries and how do they work."

[12]   "The Four Components of a Li-ion Battery," www.samsungsdi.com [Online; accessed 06/15/2021]

[13]   T. Kawamura, S. Okada, and J. ichi Yamaki, "Decomposition reaction of LiPF6-based electrolytes for lithium ion cells," *Journal of Power Sources*, vol. 156, no. 2, pp. 547–554, Jun. 2006, doi: 10.1016/j.jpowsour.2005.05.084.

[14]   V. Aravindan, J. Gnanaraj, S. Madhavi, and H. K. Liu, "Lithium-ion conducting electrolyte salts for lithium batteries," *Chemistry - A European Journal*, vol. 17, no. 51. pp. 14326–14346, Dec. 16, 2011. doi: 10.1002/chem.201101486.

[15]   J. B. Goodenough and Y. Kim, "Challenges for rechargeable Li batteries," *Chemistry of Materials*, vol. 22, no. 3. pp. 587–603, Feb. 09, 2010. doi: 10.1021/cm901452z.

[16]   Q. Wang, J. Sun, and G. Chu, "Lithium Ion Battery Fire and Explosion," 2005.

[17]   Y. T. Chen, Y. C. Chuang, J. H. Su, H. C. Yu, and Y. W. Chen-Yang, "High discharge capacity solid composite polymer electrolyte lithium battery," *Journal of Power Sources*, vol. 196, no. 5, pp. 2802–2809, Mar. 2011, doi: 10.1016/j.jpowsour.2010.11.058.

[18]   E. Bekaert, L. Buannic, U. Lassi, A. Llordés, and J. Salminen, "Electrolytes for Li- and Na-Ion Batteries: Concepts, Candidates, and the Role of Nanotechnology," in *Emerging Nanotechnologies in Rechargeable Energy Storage Systems*, Elsevier Inc., 2017, pp. 1–43. doi: 10.1016/B978-0-323-42977-1.00001-7.

CITED LITERATURE (continue)

[19]   D. M. Seo, O. Borodin, S.-D. Han, P. D. Boyle, and W. A. Henderson, "Electrolyte Solvation and Ionic Association II. Acetonitrile-Lithium Salt Mixtures: Highly Dissociated Salts," *Journal of The Electrochemical Society*, vol. 159, no. 9, Jan. 2012, doi: 10.1149/2.035209jes.

[20]   J. Andersson, "Synthesis of polycarbonate polymer electrolytes for lithium ion batteries and study of additives to raise the ionic conductivity." [Online]. Available: http://www.teknat.uu.se/student

[21]   H. P. Singh and S. S. Sekhon, "Conductivity behaviour of proton conducting polymer gel electrolytes with PVdF-HFP," *European Polymer Journal*, vol. 39, no. 1, pp. 93–98, Jan. 2003, doi: 10.1016/S0014-3057(02)00172-6.

[22]   A. Arya and A. L. Sharma, "Polymer electrolytes for lithium ion batteries: a critical study," *Ionics*, vol. 23, no. 3. Institute for Ionics, pp. 497–540, Mar. 01, 2017. doi: 10.1007/s11581-016-1908-6.

[23]   M. Galiński, A. Lewandowski, and I. Stepniak, "Ionic liquids as electrolytes," *Electrochimica Acta*, vol. 51, no. 26. Pergamon, pp. 5567–5580, Aug. 15, 2006. doi: 10.1016/j.electacta.2006.03.016.

[24]   B. Zhang *et al.*, "Mechanisms and properties of ion-transport in inorganic solid electrolytes," *Energy Storage Materials*, vol. 10. Elsevier B.V., pp. 139–159, Jan. 01, 2018. doi: 10.1016/j.ensm.2017.08.015.

[25]   X. Yao *et al.*, "All-solid-state lithium batteries with inorganic solid electrolytes: Review of fundamental science," *Chinese Physics B*, vol. 25, no. 1, Dec. 2015, doi: 10.1088/1674-1056/25/1/018802.

[26]   W. Chu *et al.*, "Understanding Ion Mobility in P2VP/NMP+I- Polymer Electrolytes: A Combined Simulation and Experimental Study," *Macromolecules*, 2020, doi: 10.1021/acs.macromol.9b02329.

[27]   L. Porcarelli, C. Gerbaldi, F. Bella, and J. R. Nair, "Super Soft All-Ethylene Oxide Polymer Electrolyte for Safe All-Solid Lithium Batteries," *Scientific Reports*, vol. 6, Jan. 2016, doi: 10.1038/srep19892.

CITED LITERATURE (continue)

[28]   A. M. Gaikwad, D. A. Steingart, T. Nga Ng, D. E. Schwartz, and G. L. Whiting, "A flexible high potential printed battery for powering printed electronics," *Applied Physics Letters*, vol. 102, no. 23, Jun. 2013, doi: 10.1063/1.4810974.

[29]   S. H. Huang, P. Liu, A. Mokasdar, and L. Hou, "Additive manufacturing and its societal impact: a literature review," *The International Journal of Advanced Manufacturing Technology*, vol. 67, no. 5–8, Jul. 2013, doi: 10.1007/s00170-012-4558-5.

[30]   K. Sun, T.-S. Wei, B. Y. Ahn, J. Y. Seo, S. J. Dillon, and J. A. Lewis, "3D Printing of Interdigitated Li-Ion Microbattery Architectures," *Advanced Materials*, vol. 25, no. 33, Sep. 2013, doi: 10.1002/adma.201301036.

[31]   "Rheological Properties," in *Food Physics*, Berlin, Heidelberg: Springer Berlin Heidelberg. doi: 10.1007/978-3-540-34194-9_4.

[32]   "Rheology 101- - Learning the Basics," www.azom.com [Online; accessed 05/25/2021]

[33]   "Viscoelasticity and dynamic mechanical testing A. Franck, TA Instruments Germany."

[34]   M. Cheng *et al.*, "Elevated-Temperature 3D Printing of Hybrid Solid-State Electrolyte for Li-Ion Batteries," *Advanced Materials*, vol. 30, no. 39, Sep. 2018, doi: 10.1002/adma.201800615.

[35]   M. B. Armand, "POLYMER ELECTROLYTES," 1986. www.annualreviews.org [Online; Accessed 05/31/2021].

[36]   X. Feng, M. Ouyang, X. Liu, L. Lu, Y. Xia, and X. He, "Thermal runaway mechanism of lithium ion battery for electric vehicles: A review," *Energy Storage Materials*, vol. 10. Elsevier B.V., pp. 246–267, Jan. 01, 2018. doi: 10.1016/j.ensm.2017.05.013.

[37]   G. P. Beauregard, "REPORT OF INVESTIGATION: HYBRIDS PLUS PLUG IN HYBRID ELECTRIC VEHICLE Revision 1," 2008.

[38]   S. Zhang, Q. Zhou, and Y. Xia, "Influence of Mass Distribution of Battery and Occupant on Crash Response of Small Lightweight Electric Vehicle," Apr. 2015. doi: 10.4271/2015-01-0575.

CITED LITERATURE (continue)

[39]   R. Spotnitz and J. Franklin, "Abuse behavior of high-power, lithium-ion cells," *Journal of Power Sources*, vol. 113, no. 1, pp. 81–100, Jan. 2003, doi: 10.1016/S0378-7753(02)00488-3.

[40]   Y. Saito, K. Takano, and A. Negishi, "Thermal behaviors of lithium-ion cells during overcharge," *Journal of Power Sources*, vol. 97–98, Jul. 2001, doi: 10.1016/S0378-7753(01)00703-0.

[41]   J. Wen, Y. Yu, and C. Chen, "A Review on Lithium-Ion Batteries Safety Issues: Existing Problems and Possible Solutions," *Materials Express*, vol. 2, no. 3, Sep. 2012, doi: 10.1166/mex.2012.1075.

[42]   M. Ouyang *et al.*, "Overcharge-induced capacity fading analysis for large format lithium-ion batteries with LiyNi1/3Co1/3Mn1/3O2 + LiyMn2O4 composite cathode," *Journal of Power Sources*, vol. 279, pp. 626–635, Apr. 2015, doi: 10.1016/j.jpowsour.2015.01.051.

[43]   H.-F. LI, J.-K. GAO, and S.-L. ZHANG, "Effect of Overdischarge on Swelling and Recharge Performance of Lithium Ion Cells," *Chinese Journal of Chemistry*, vol. 26, no. 9, Sep. 2008, doi: 10.1002/cjoc.200890286.

[44]   S. Erol, M. E. Orazem, and R. P. Muller, "Influence of overcharge and over-discharge on the impedance response of LiCoO 2 | C batteries," *Journal of Power Sources*, vol. 270, pp. 92–100, Dec. 2014, doi: 10.1016/j.jpowsour.2014.07.038.

[45]   L. Zhang *et al.*, "Capacity fading mechanism during long-term cycling of over-discharged LiCoO2/mesocarbon microbeads battery," *Journal of Power Sources*, vol. 293, pp. 1006–1015, Jun. 2015, doi: 10.1016/j.jpowsour.2015.06.040.

[46]   Y. Zheng, X. Han, L. Lu, J. Li, and M. Ouyang, "Lithium ion battery pack power fade fault identification based on Shannon entropy in electric vehicles," *Journal of Power Sources*, vol. 223, pp. 136–146, Feb. 2013, doi: 10.1016/j.jpowsour.2012.09.015.

[47]   D. H. Doughty, "Vehicle Battery Safety Roadmap Guidance," Golden, CO (United States), Oct. 2012. doi: 10.2172/1055366.

[48]   Q. Wang, J. Sun, X. Yao, and C. Chen, "Thermal stability of LiPF6/EC + DEC electrolyte with charged electrodes for lithium ion batteries," *Thermochimica Acta*, vol. 437, no. 1–2, pp. 12–16, Oct. 2005, doi: 10.1016/j.tca.2005.06.010.

CITED LITERATURE (continue)

[49]   R. Spotnitz and J. Franklin, "Abuse behavior of high-power, lithium-ion cells," *Journal of Power Sources*, vol. 113, no. 1, pp. 81–100, Jan. 2003, doi: 10.1016/S0378-7753(02)00488-3.

[50]   M. N. Richard and J. R. Dahn, "Accelerating Rate Calorimetry Study on the Thermal Stability of Lithium Intercalated Graphite in Electrolyte. I. Experimental," *Journal of The Electrochemical Society*, vol. 146, no. 6, Jun. 1999, doi: 10.1149/1.1391893.

[51]   J. ichi Yamaki, H. Takatsuji, T. Kawamura, and M. Egashira, "Thermal stability of graphite anode with electrolyte in lithium-ion cells," in *Solid State Ionics*, Jun. 2002, vol. 148, no. 3–4, pp. 241–245. doi: 10.1016/S0167-2738(02)00060-7.

[52]   J. Jiang and J. R. Dahn, "ARC studies of the thermal stability of three different cathode materials: LiCoO2; Li[Ni0.1Co0.8Mn0.1]O 2; and LiFePO4, in LiPF6 and LiBoB EC/DEC electrolytes," *Electrochemistry Communications*, vol. 6, no. 1, pp. 39–43, Jan. 2004, doi: 10.1016/j.elecom.2003.10.011.

[53]   S. Al-Saadi, P. C. Banerjee, M. R. Anisur, and R. K. S. Raman, "Hexagonal Boron Nitride Impregnated Silane Composite Coating for Corrosion Resistance of Magnesium Alloys for Temporary Bioimplant Applications," *Metals*, vol. 7, no. 12, Nov. 2017, doi: 10.3390/met7120518.

[54]   G. W. Lee, M. Park, J. Kim, J. I. Lee, and H. G. Yoon, "Enhanced thermal conductivity of polymer composites filled with hybrid filler," *Composites Part A: Applied Science and Manufacturing*, vol. 37, no. 5, pp. 727–734, May 2006, doi: 10.1016/j.compositesa.2005.07.006.

[55]   S. P. Ogilvie *et al.*, "Considerations for spectroscopy of liquid-exfoliated 2D materials: emerging photoluminescence of N-methyl-2-pyrrolidone," *Scientific Reports*, vol. 7, no. 1, Dec. 2017, doi: 10.1038/s41598-017-17123-5.

[56]   "NMP/N-Methyl-2-Pyrrolidone," en.wikipedia.org [Online; Accessed 06/02/2021].

[57]   G. dong Kang and Y. ming Cao, "Application and modification of poly(vinylidene fluoride) (PVDF) membranes - A review," *Journal of Membrane Science*, vol. 463. Elsevier, pp. 145–165, Aug. 01, 2014. doi: 10.1016/j.memsci.2014.03.055.

[58]   J. W. Fergus, "Ceramic and polymeric solid electrolytes for lithium-ion batteries," *Journal of Power Sources*, vol. 195, no. 15. Elsevier, pp. 4554–4569, Aug. 01, 2010. doi: 10.1016/j.jpowsour.2010.01.076.

CITED LITERATURE (continue)

[59]   J. Kalhoff, D. Bresser, M. Bolloli, F. Alloin, J.-Y. Sanchez, and S. Passerini, "Enabling LiTFSI-based Electrolytes for Safer Lithium-Ion Batteries by Using Linear Fluorinated Carbonates as (Co)Solvent," *ChemSusChem*, vol. 7, no. 10, Oct. 2014, doi: 10.1002/cssc.201402502.

[60]   H. Yang, K. Kwon, T. M. Devine, and J. W. Evans, "Aluminum Corrosion in Lithium Batteries An Investigation Using the Electrochemical Quartz Crystal Microbalance," *Journal of The Electrochemical Society*, vol. 147, no. 12, 2000, doi: 10.1149/1.1394077.

[61]   A. Arya and A. L. Sharma, "Polymer electrolytes for lithium ion batteries: a critical study," *Ionics*, vol. 23, no. 3, Mar. 2017, doi: 10.1007/s11581-016-1908-6.

[62]   "1-ETHYL-3-METHYLIMIDAZOLIUM BIS(TRIFLUOROMETHYLSULFONYL)IMIDE, 99% [EMIIM]," Jun. 07, 2021.

[63]   M. Armand, F. Endres, D. R. MacFarlane, H. Ohno, and B. Scrosati, "Ionic-liquid materials for the electrochemical challenges of the future," *Nature Materials*, vol. 8, no. 8, Aug. 2009, doi: 10.1038/nmat2448.

[64]   S. Ryu, H. Oh, and J. Kim, "Facile Liquid-Exfoliation Process of Boron Nitride Nanosheets for Thermal Conductive Polyphthalamide Composite," *Polymers*, vol. 11, no. 10, Oct. 2019, doi: 10.3390/polym11101628.

[65]   "Nordson EFD - General Purpose Tips," www.nordson.com Jun. [Online; Accessed 06/10/2021].

[66]   G. Bieker, M. Winter, and P. Bieker, "Electrochemical in situ investigations of SEI and dendrite formation on the lithium metal anode," *Physical Chemistry Chemical Physics*, vol. 17, no. 14, 2015, doi: 10.1039/C4CP05865H.

[67]   K.-H. Chen *et al.*, "Dead lithium: mass transport effects on voltage, capacity, and failure of lithium metal anodes," *Journal of Materials Chemistry A*, vol. 5, no. 23, 2017, doi: 10.1039/C7TA00371D.

[68]   "Coulombic and Energy Efficiency with the Battery," Jun. 10, 2021.

CITED LITERATURE (continue)

[69] H. Wang *et al.*, "Interface Properties between Lithium Metal and a Composite Polymer Electrolyte of PEO18Li(CF3SO2)2N-Tetraethylene Glycol Dimethyl Ether," *Membranes*, vol. 3, no. 4, Oct. 2013, doi: 10.3390/membranes3040298.

[70] "Battery Capacity," www.pveducation.org [Online; Accessed 06/10/2021].

VITA

NAME:

Massimiliano Mastrogiorgio

EDUCATION:

B.S., Energy engineering, Politecnico di Torino, Turin, Italy, 2019

M.S., Mechanical Engineering, University of Illinois at Chicago, Chicago, Illinois, 2021

M.S., Energy and Nuclear Engineering, Politecnico di Torino, Turin, Italy, 2021

ACADEMIC EXPERIENCE:

Department of Mechanical and Industrial Engineering (M.S. Thesis), University of Illinois at Chicago, Chicago, Illinois: Nano Engineering Lab, 2021

Energy and Nuclear department (B.S. Thesis), Politecnico di Torino, Turin, Italy, 2021

ACHIEVEMENTS:

One of the seven top Energy and Mechanical Engineering students of the TOP-UIC double master's degree program, based on B.S. education outcomes (Scholarship from Politecnico di Torino)